Cell Reports
Medicine

Article

USP9X mediates an acute adaptive response to MAPK suppression in pancreatic cancer but creates multiple actionable therapeutic vulnerabilities

Graphical abstract

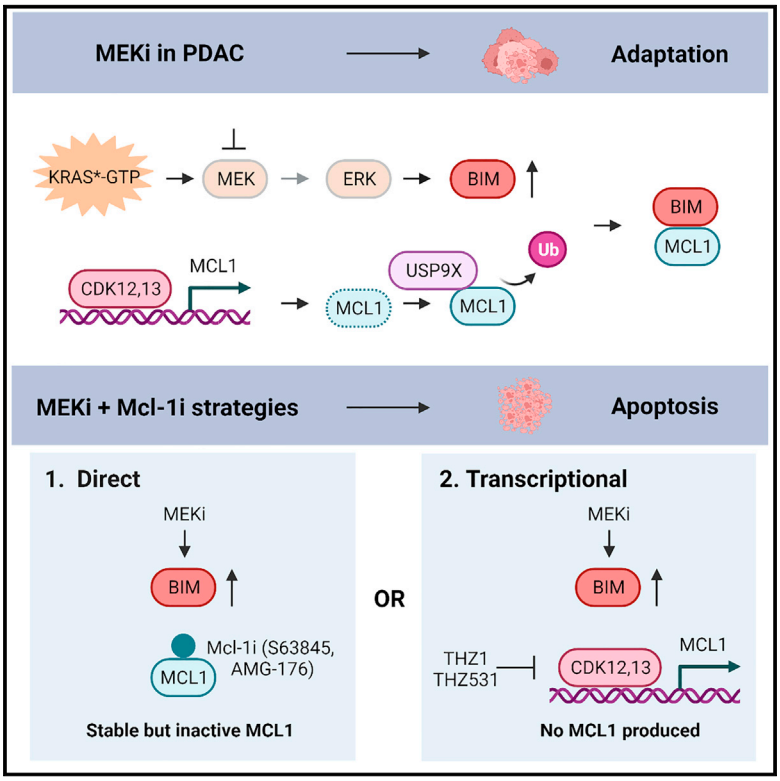

Highlights

- Mcl-1 upregulation is an adaptive response to MEK inhibition in PDAC
- MEK inhibitors acutely stabilize Mcl-1 protein by inducing Mcl-1:USP9X complexes
- Combined MEK/Mcl-1 inhibitors trigger dramatic tumor regression in PDACs
- MEK/CDK inhibition represents a second promising therapeutic strategy for PDACs

Authors

Naiara Perurena, Rebecca Lock, Rachel A. Davis, ..., Owen J. Sansom, Andrew J. Aguirre, Karen Cichowski

Correspondence

kcichowski@rics.bwh.harvard.edu

In brief

Perurena et al. show that PDACs are resistant to MEK inhibitors because they trigger the formation of USP9X:Mcl-1 complexes, thereby acutely stabilizing Mcl-1 and inhibiting apoptosis. Resistance can be overcome by targeting Mcl-1 with direct inhibitors or by suppressing Mcl-1 transcription with CDK inhibitors, revealing new therapeutic strategies for PDAC.

Perurena et al., 2023, Cell Reports Medicine *4*, 101007
April 18, 2023 © 2023
https://doi.org/10.1016/j.xcrm.2023.101007

CellPress

Please cite this article in press as: Perurena et al., USP9X mediates an acute adaptive response to MAPK suppression in pancreatic cancer but creates multiple actionable therapeutic vulnerabilities, Cell Reports Medicine (2023), https://doi.org/10.1016/j.xcrm.2023.101007

Cell Reports Medicine

CellPress
OPEN ACCESS

Article

USP9X mediates an acute adaptive response to MAPK suppression in pancreatic cancer but creates multiple actionable therapeutic vulnerabilities

Naiara Perurena,[1,2,3,4] Rebecca Lock,[1,2,3] Rachel A. Davis,[1,2] Srivatsan Raghavan,[2,3,5,6] Natalie F. Pilla,[1,2] Raymond Ng,[5,6] Patrick Loi,[1,2,3] Caroline J. Guild,[1,2] Abigail L. Miller,[1,2,3] Ewa Sicinska,[7] James M. Cleary,[3,5] Douglas A. Rubinson,[3,5] Brian M. Wolpin,[3,5] Nathanael S. Gray,[8] Sandro Santagata,[3,4,9] William C. Hahn,[2,3,5,6] Jennifer P. Morton,[10,11] Owen J. Sansom,[10,11] Andrew J. Aguirre,[2,3,5,6] and Karen Cichowski[1,2,3,4,12,*]

[1]Genetics Division, Brigham and Women's Hospital, Boston, MA 02115, USA
[2]Department of Medicine, Brigham and Women's Hospital, Boston, MA 02115, USA
[3]Harvard Medical School, Boston, MA 02115, USA
[4]Ludwig Center at Harvard, Boston, MA 02115, USA
[5]Department of Medical Oncology, Dana-Farber Cancer Institute, Boston, MA 02215, USA
[6]Broad Institute of MIT and Harvard, Cambridge, MA 02142, USA
[7]Department of Oncologic Pathology, Dana Farber Cancer Institute, Boston, MA 02115, USA
[8]Department of Chemical and Systems Biology, Chem-H and Stanford Cancer Institute, Stanford University, Stanford, CA 94305, USA
[9]Department of Pathology, Brigham and Women's Hospital, Boston, MA 02115, USA
[10]Cancer Research UK Beatson Institute, Switchback Road, Bearsden, Glasgow G61 1BD, UK
[11]Institute of Cancer Sciences, University of Glasgow, Switchback Road, Glasgow G11 1QH, UK
[12]Lead contact
*Correspondence: kcichowski@rics.bwh.harvard.edu
https://doi.org/10.1016/j.xcrm.2023.101007

SUMMARY

Pancreatic ductal adenocarcinomas (PDACs) frequently harbor *KRAS* mutations. Although MEK inhibitors represent a plausible therapeutic option, most PDACs are innately resistant to these agents. Here, we identify a critical adaptive response that mediates resistance. Specifically, we show that MEK inhibitors upregulate the anti-apoptotic protein Mcl-1 by triggering an association with its deubiquitinase, USP9X, resulting in acute Mcl-1 stabilization and protection from apoptosis. Notably, these findings contrast the canonical positive regulation of Mcl-1 by RAS/ERK. We further show that Mcl-1 inhibitors and cyclin-dependent kinase (CDK) inhibitors, which suppress Mcl-1 transcription, prevent this protective response and induce tumor regression when combined with MEK inhibitors. Finally, we identify USP9X as an additional potential therapeutic target. Together, these studies (1) demonstrate that USP9X regulates a critical mechanism of resistance in PDAC, (2) reveal an unexpected mechanism of Mcl-1 regulation in response to RAS pathway suppression, and (3) provide multiple distinct promising therapeutic strategies for this deadly malignancy.

INTRODUCTION

Pancreatic ductal adenocarcinoma (PDAC) is one of the deadliest malignancies with a 5-year survival rate of less than 8%.[1] Most individuals diagnosed with PDAC present with advanced disease and are typically treated with palliative chemotherapy that prolongs median survival by a few months.[2] Over 90% of PDACs are driven by activating mutations in *KRAS*;[3] however, there are still no effective targeted therapies for these *KRAS*-driven malignancies.

Drugs that covalently target $KRAS^{G12C}$ mutations have recently been approved for the treatment of non-small cell lung cancers;[4] however, this mutant allele is uncommon in PDAC. Unfortunately, trials with agents that inhibit the downstream effector, MEK, have been disappointing in PDAC and other RAS-driven cancers,[5,6] although it is still unclear why many of these tumors are refractory to MEK inhibition. For example, it is well known that RAS/ERK activation triggers proteasomal destruction of the pro-apoptotic protein Bim; conversely, MEK inhibitors upregulate Bim in *KRAS*-mutant tumor cells through effects on stability and transcription.[7–9] Similarly, ERK has been shown to stabilize the Mcl-1 protein and increase its expression via transcriptional mechanisms, whereas MEK/ERK suppression reduces Mcl-1 levels.[10–14] These observations are consistent with a positive relationship between oncogenic RAS and pro-survival pathways but further confound the observed resistance to MEK inhibitors.

Therapeutic resistance can be conferred by genetic alterations or dynamic adaptation of cell signaling pathways. Because potent pro-apoptotic signals are known to be activated in response to MEK suppression, we investigated whether direct changes in pro-survival proteins might mediate resistance to

This is an open access article under the CC BY-NC-ND license (http://creativecommons.org/licenses/by-nc-nd/4.0/).

Please cite this article in press as: Perurena et al., USP9X mediates an acute adaptive response to MAPK suppression in pancreatic cancer but creates multiple actionable therapeutic vulnerabilities, Cell Reports Medicine (2023), https://doi.org/10.1016/j.xcrm.2023.101007

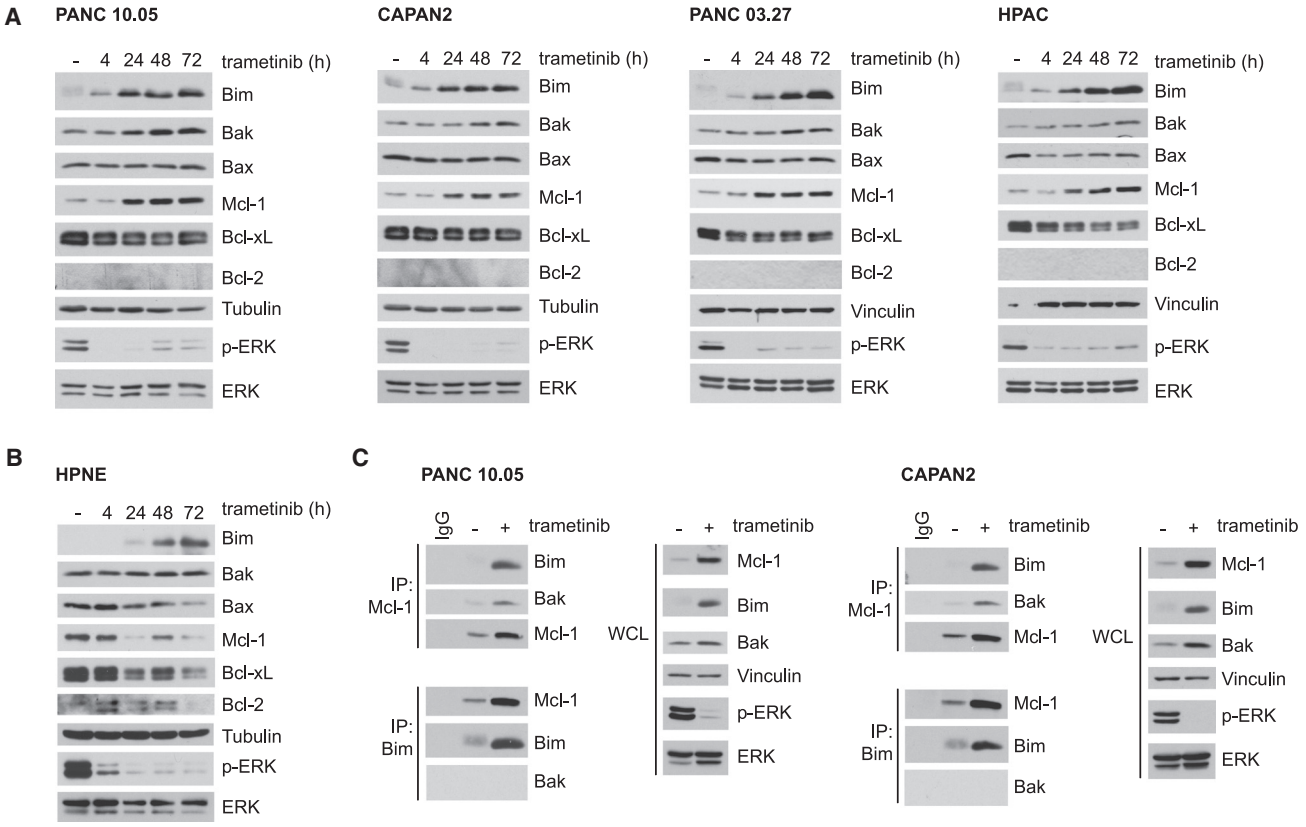

Figure 1. MEK inhibitors induce Mcl-1 protein expression in PDACs

(A) Western blots depicting changes in the levels of Bcl-2-family member proteins in PDAC cell lines following treatment with 25 nM trametinib for the indicated times.

(B) Western blots depicting levels of Bcl-2 family members in HPNE cells following treatment with 50 nM trametinib for the indicated times.

(C) Immunoprecipitation (IP) demonstrating interactions of Mcl-1 with Bim and Bak following MEK inhibition (48 h trametinib) in PANC 10.05 and CAPAN2 cells. WCL, whole-cell lysate.

these agents in PDACs. Here we report that MEK inhibitors trigger a potent adaptive response in PDACs by acutely stabilizing the Mcl-1 protein. Mechanistic studies further reveal that this protective response confers new dependencies on USP9X, Mcl-1, and cyclin-dependent kinases (CDKs). Based on this insight, we demonstrate the potent efficacy of two distinct MEK inhibitor-based drug combinations in PDAC cells, human tumor organoids, and multiple *in vivo* models. Notably, the decision to target specific proteins in different tumor types is often guided by standard dependency screens. However, the findings presented here suggest that treatment-induced dependencies may be missed by relying on this approach and highlight the need to deconstruct how various tumor types differentially adapt to single agents so that we may develop more effective treatments.

RESULTS

MEK inhibitors potently induce Mcl-1 protein expression in PDACs

In normal cells, Ras pathway activation suppresses the expression of pro-apoptotic Bcl-2-family proteins, such as Bim, and simultaneously increases the anti-apoptotic protein Mcl-1 by enhancing its transcription and stability.[14,15] Accordingly, MEK inhibitors typically reverse these effects, increasing Bim and decreasing Mcl-1 expression.[7,9,16–19] Therefore, it is not fully understood why MEK inhibitors cannot trigger apoptosis in many RAS-driven tumor types. To investigate this question in pancreatic cancer, we examined the expression of pro-survival Bcl-2 family members (Mcl-1, Bcl-xL, and Bcl-2) and pro-apoptotic proteins (Bim, Bak, and Bax) in response to the MEK inhibitor trametinib over 72 h. Consistent with previous observations, Bim levels increased in all of the PDAC cell lines over time (PANC 10.05, CAPAN2, PANC 03.27, and HPAC) and in non-transformed, immortalized human pancreatic cells (HPNE cells) (Figures 1A and 1B). A slight increase in the pro-apoptotic effector protein Bak was also observed. However, the most striking difference was the dynamic pattern of Mcl-1 expression. Whereas trametinib decreased Mcl-1 levels in non-transformed HPNE cells as expected (Figure 1B), Mcl-1 expression increased in all of the PDAC cell lines following trametinib treatment (Figure 1A). The kinetics of Mcl-1 induction were delayed; protein levels remained low after 4 h of exposure to trametinib but were substantially elevated within 24 h. The rate of Mcl-1

Please cite this article in press as: Perurena et al., USP9X mediates an acute adaptive response to MAPK suppression in pancreatic cancer but creates multiple actionable therapeutic vulnerabilities, Cell Reports Medicine (2023), https://doi.org/10.1016/j.xcrm.2023.101007

CellPress
OPEN ACCESS

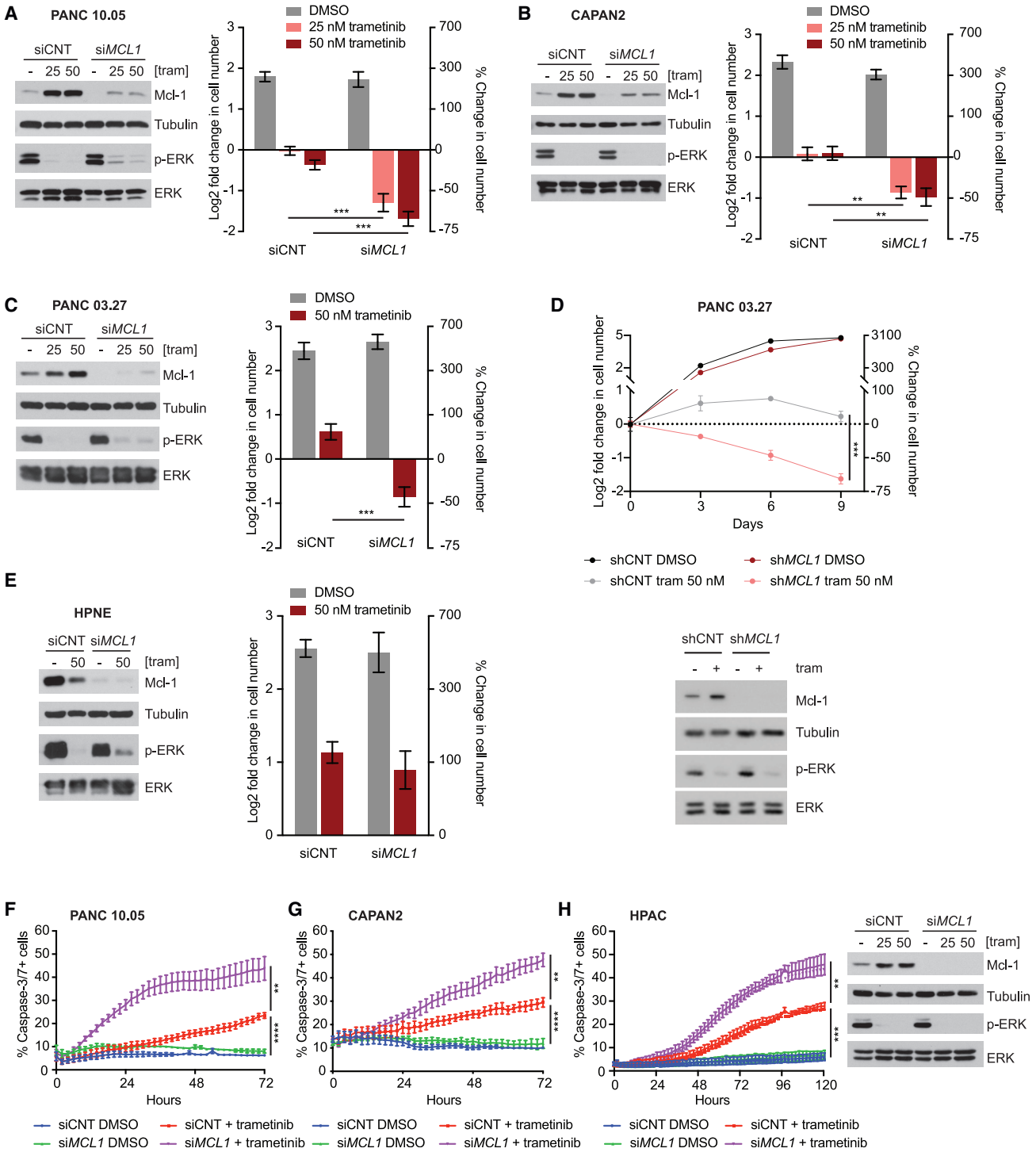

Figure 2. MEK inhibitors trigger an adaptive dependency on Mcl-1 in PDACs

(A–C) Western blots: levels of Mcl-1 in PDAC cell lines following siRNA-mediated knockdown and treatment with the indicated concentration (nM) of trametinib (tram) for 48 h. Graphs: log2 fold change (left y axis) and percent change (right y axis) in cell number in si*MCL1* or siCNT PDAC cells treated with tram for 72 h (mean ± SD of technical replicates, n = 3; $^{**}p < 0.01$, $^{***}p < 0.001$).

(D) Graph: log2 fold change (left y axis) and percent change (right y axis) in cell numbers in sh*MCL1* or shCNT PANC 03.27 cells during 9 days of 50 nM tram treatment (mean ± SD of technical replicates, n = 3; $^{***}p < 0.0001$, unpaired t test). Western blots: levels of Mcl-1 in PANC 03.27 cells following shRNA-mediated knockdown and treatment with 50 nM tram for 48 h.

(legend continued on next page)

Please cite this article in press as: Perurena et al., USP9X mediates an acute adaptive response to MAPK suppression in pancreatic cancer but creates multiple actionable therapeutic vulnerabilities, Cell Reports Medicine (2023), https://doi.org/10.1016/j.xcrm.2023.101007

upregulation varied slightly, but maximal induction was observed between 24 and 72 h, depending on the cell line (Figure 1A). Mcl-1 was the only protein that increased among anti-apoptotic family members, whereas Bcl-xL levels did not change or were reduced in PDAC and HPNE cells (Figures 1A and 1B). The Bcl-2 protein was not expressed in PDAC cells and did not increase in the presence of trametinib (Figure 1A; CCLE, cBioportal).

To determine whether the induction of Mcl-1 resulted in a concomitant increase in binding to pro-apoptotic family members, Mcl-1 and Bim were immunoprecipitated from PDAC cells. Notably, trametinib induced the formation of Mcl-1:Bim and Mcl-1:Bak complexes in multiple PDAC cell lines (Figure 1C). Together, these results demonstrate that, while MEK suppression reduces Mcl-1 levels in non-transformed cells and some cancers, as reported previously,[7,16–19] MEK inhibitors substantially increase Mcl-1 levels and its association with pro-apoptotic proteins in PDACs, suggesting a more complex relationship between the RAS/ERK pathway and apoptotic signaling in this tumor type. These observations also raised the intriguing possibility that Mcl-1 induction might serve an important protective response to MEK inhibitors in pancreatic cancer.

MEK inhibitors trigger an adaptive dependency on Mcl-1 in pancreatic cancers

According to CRISPR dependency data, PDAC cells appear to be a largely Mcl-1-independent lineage (depmap.org; Figure S1A). Therefore, based on these observations alone, Mcl-1 inhibitors would not be expected to be effective in pancreatic cancer. However, because MEK inhibitors potently induced Mcl-1 expression, we hypothesized that these agents might sensitize pancreatic cancers to Mcl-1 depletion. To investigate this possibility, *MCL1* was genetically depleted by small interfering RNAs (siRNAs), and cells were treated with trametinib. Consistent with Dependency Map data, siRNA-mediated suppression of Mcl-1 alone did not affect cell proliferation (Figures 2A–2C and S1B). However, trametinib dramatically sensitized PDAC cells to Mcl-1 depletion, resulting in loss of 45%–70% of cells after only 72 h of treatment (Figures 2A–2C). Similar responses were observed when Mcl-1 was ablated by shRNAs and CRISPR sgRNAs (Figures 2D and S1C). Importantly, cell numbers continued to decrease over time in response to combined MEK/Mcl-1 suppression, as illustrated by longer-term assays (Figures 2D and S1C), whereas stable loss of Mcl-1 alone had no effect on PDAC proliferation. By contrast, trametinib reduced the proliferation of non-transformed HPNE cells, but Mcl-1 loss did not further enhance these effects (Figure 2E).

To confirm that PDAC cells were dying via apoptosis, caspase-3 and -7 activity was measured over time using live-cell imaging. Suppression of Mcl-1 expression alone had no effect on caspase activity in PANC 10.05, CAPAN2, and HPAC cells (Figures 2F–2H). Trametinib induced low levels of apoptosis compared to DMSO-treated cells; however, in Mcl-1-depleted cells, trametinib triggered apoptosis in ~40%–50% of the cells within 72 h (Figures 2F–2H). Non-transformed HPNE cells showed no apoptotic response to trametinib or *siMCL1*, alone or together (Figure S1D). To confirm that this was due to a lack of sensitivity to *siMCL1*/trametinib and not due to intrinsic defects in apoptosis, HPNE cells were treated with staurosporine, which induced potent caspase activation in *siCNT* and *siMCL1* cells (Figure S1D). These results demonstrate that acute upregulation of Mcl-1 in response to MEK inhibition functions as an adaptive resistance mechanism that suppresses apoptosis by binding to pro-apoptotic family members. However, this consequently triggers a therapeutic vulnerability; while PDACs are normally Mcl-1 independent, MEK inhibitors render these cells sensitive to Mcl-1 depletion. While the suppression of MEK and Bcl-2 family member inhibitors has been shown to cooperate in other tumor types, the mechanisms that underlie this cooperativity have largely remained elusive.[20–22] Therefore, we sought to further deconstruct this dynamic mechanism of resistance and identify other regulatory components, in part, to identify additional therapeutic targets in PDAC.

MEK inhibitors acutely stabilize Mcl-1 protein

Because the RAS/ERK pathway has been reported to positively regulate Mcl-1 expression in other settings, through effects on transcription and protein stability,[8,15] these observations were particularly surprising. Therefore, to elucidate the mechanism by which suppression of this pathway induced Mcl-1 upregulation in PDACs, we first examined *MCL1* mRNA levels in PANC 10.05, CAPAN2, and non-transformed HPNE cells. In HPNE cells, *MCL1* transcript levels were reduced in response to trametinib, consistent with the canonical positive relationship between ERK and *MCL1* transcription (Figure 3A). In pancreatic cancer cells, *MCL1* transcript levels either did not substantially change or slightly decreased (Figure 3B). Therefore, while the ~50% suppression of *MCL1* transcript levels likely contributes to the reduction of Mcl-1 protein in HPNE cells (Figure 1B), the mRNA expression pattern in PDAC cells does not explain the unexpected increase in Mcl-1 protein in response to trametinib.

In a subset of tumor types, Mcl-1 translation is regulated by mTOR.[23] Specifically, mTOR kinase inhibitors decrease Mcl-1 levels in colorectal cancers that have become dependent on mTORC1.[23] In addition, MEK inhibitors can induce feedback activation of the AKT/mTORC1 pathway in some settings. Therefore, we investigated whether the increase in Mcl-1 expression in response to trametinib might be due to feedback activation of AKT/mTORC1 and enhanced Mcl-1 translation. However, phospho-AKT and phospho-S6 levels did not increase in response to trametinib (Figures 3C and 3D). Moreover, neither the addition of the AKT inhibitor MK2206 nor the mTOR kinase inhibitor

(E) Western blots: levels of Mcl-1 in HPNE cells following siRNA-mediated knockdown and treatment with 50 nM tram for 48 h. Graph: log2 fold change (left y axis) and percent change (right y axis) in cell numbers in si*MCL1* or siCNT HPNE cells treated with 50 nM tram for 72 h (mean ± SD of technical replicates, n = 3).
(F–H) Graphs: CC3/7 activation kinetics in si*MCL1* or siCNT PANC 10.05, CAPAN2, and HPAC cells treated with 25 nM tram. Graphs depict the average percentage of nuclei that are co-positive for activated CC3/7 (mean ± SEM of biological replicates, n = 4; $^{**}p < 0.01$, $^{***}p < 0.001$, $^{****}p < 0.0001$). Western blots: levels of Mcl-1 in HPAC cells following *MCL1* knockdown (si*MCL1)* and treatment with the indicated concentrations (nM) of tram for 48 h.
See also Figures S1B–S1D.

Please cite this article in press as: Perurena et al., USP9X mediates an acute adaptive response to MAPK suppression in pancreatic cancer but creates multiple actionable therapeutic vulnerabilities, Cell Reports Medicine (2023), https://doi.org/10.1016/j.xcrm.2023.101007

CellPress
OPEN ACCESS

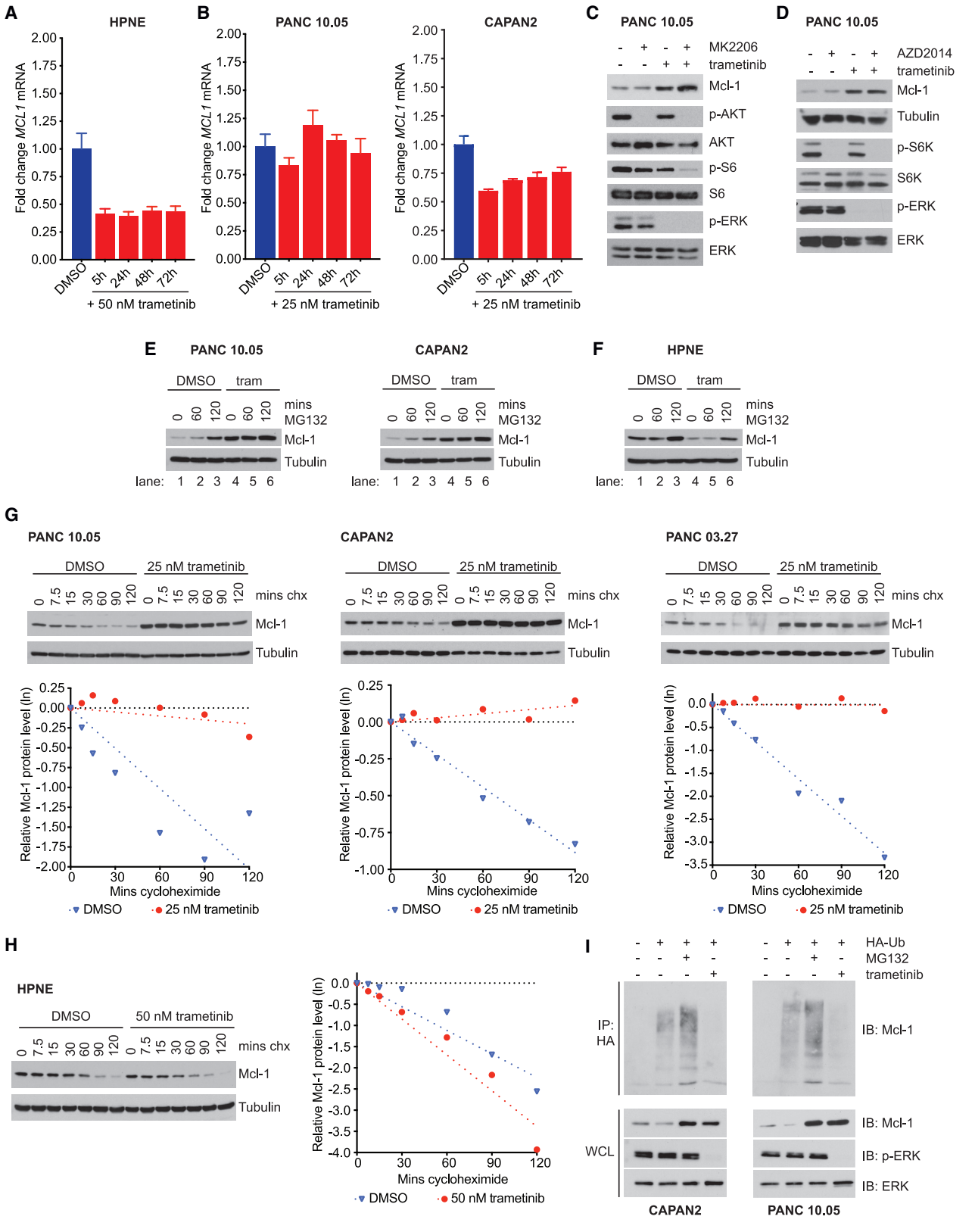

(legend on next page)

Please cite this article in press as: Perurena et al., USP9X mediates an acute adaptive response to MAPK suppression in pancreatic cancer but creates multiple actionable therapeutic vulnerabilities, Cell Reports Medicine (2023), https://doi.org/10.1016/j.xcrm.2023.101007

AZD2014 suppressed induction of Mcl-1 in response to trametinib (Figures 3C and 3C), demonstrating that these effects were not caused by enhanced Mcl-1 translation by mTORC1 or by another AKT-dependent process. In this respect, PDAC tumors are more similar to *KRAS*-mutant NSCLCs, where Mcl-1 expression is also not regulated by mTORC1, as opposed to colon cancers, where Mcl-1 is more mTORC1 dependent.[23]

Unlike other anti-apoptotic family members, Mcl-1 has a short protein half-life. Consequently, changes in Mcl-1 stability have a major effect on Mcl-1 levels.[24] To determine whether trametinib was affecting Mcl-1 stability, we first assessed the effects of the proteasome inhibitor MG132 in the presence or absence of trametinib. Acute treatment with MG132 increased Mcl-1 protein levels in PDAC cell lines, confirming that Mcl-1 is relatively unstable in these cancers under basal conditions (Figure 3E, lanes 1–3). By contrast, cells exposed to trametinib exhibited an increase in Mcl-1 levels, which was not further enhanced by MG132 (Figure 3E, lanes 4–6), suggesting that trametinib was already maximally suppressing proteasomal degradation of Mcl-1. Conversely, in HPNE cells, MG132 increased Mcl-1 levels in the presence and absence of trametinib, indicating that Mcl-1 was undergoing proper proteasomal degradation in both settings and illustrating the differential effect of trametinib on Mcl-1 in PDAC versus non-transformed pancreatic cells (Figure 3F). However, to firmly establish a role of protein stabilization in this response, cycloheximide (CHX) chase assays were performed in PDAC and HPNE cell lines. While Mcl-1 was rapidly degraded in the absence of trametinib in all cell lines (Figures 3G and 3H), Mcl-1 was potently stabilized by trametinib in PDAC cells (Figure 3G). This was not the case in HPNE cells, where Mcl-1 remained equally labile in the presence and absence of trametinib (Figure 3H).

These results suggested that the induction of Mcl-1 triggered by MEK inhibitors in PDACs is due to an increase in its stability, likely caused by a decrease in its ubiquitin-mediated degradation. To directly examine Mcl-1 ubiquitination, PDAC cells were transfected with hemagglutinin (HA)-tagged ubiquitin (HA-Ub), which was then immunoprecipitated from cells in the presence or absence of trametinib. Mcl-1 immunoblots revealed a higher-mobility protein smear in untreated cells, corresponding to ubiquitinated Mcl-1, which was further enhanced by MG132 treatment (Figure 3I). However, trametinib potently suppressed Mcl-1 ubiquitination while triggering an increase in total Mcl-1 protein levels comparable to those observed in MG132-treated cells (Figure 3I). Taken together, these findings demonstrate that MEK inhibitors acutely increase Mcl-1 levels in PDACs by inhibiting its ubiquitination and subsequent degradation by the proteasome.

Trametinib-induced Mcl-1 stabilization is regulated by USP9X

In hematopoietic malignancies, Mcl-1 is regulated by USP9X, which deubiquitinates and consequently stabilizes the Mcl-1 protein.[25] To determine whether USP9X might be involved in the dynamic stabilization of Mcl-1 in response to trametinib, three distinct shRNA sequences were used to ablate USP9X expression in PANC 10.05 cells. As shown throughout, trametinib and MG132 increased Mcl-1 protein levels in PDAC cells (Figure 4A, lanes 1–4); however, USP9X depletion reversed the effects of trametinib, nearly restoring Mcl-1 to the low, baseline expression levels observed in untreated cells (Figure 4A, lanes 5, 7, and 9). Importantly, proteasome inhibitors counteracted the effects of USP9X suppression, suggesting that USP9X loss was functioning by decreasing Mcl-1 protein stability (Figure 4A, lanes 6, 8, and 10). These findings were confirmed in PANC 03.27 cells (Figure 4B) and by USP9X siRNAs (Figure 4C).

To directly examine the role of USP9X in Mcl-1 stability in response to MEK inhibition, CHX degradation assays were performed in PANC 10.05 and PANC 03.27 cells. In the absence of trametinib, Mcl-1 was degraded at similar rapid rates in sh*USP9X*-expressing cells and those expressing control shRNA sequences (shCNT) (Figures 4D and S2). However, while trametinib stabilized Mcl-1 in shCNT cells, Mcl-1 protein remained unstable in sh*USP9X*-expressing cells in the presence of trametinib (Figures 4D and S2).

Finally, we reasoned that if USP9X-mediated stabilization of Mcl-1 was a critical mechanism of adaptation, then MEK inhibitors should ultimately kill USP9X-deficient PDACs. As shown in Figure 4E, approximately 50% of PDAC cells died within 72 h in response to trametinib when USP9X was ablated. Moreover, chemical USP9X inhibition completely prevented Mcl-1 stabilization in response to MEK inhibition and induced potent cell death when combined with trametinib (Figure 4F). Incidentally, these observations suggest that USP9X may also represent a potential therapeutic target in this tumor type. Regardless, they demonstrate that USP9X plays an indispensable role in the adaptive resistance of PDACs to MEK inhibitors by regulating Mcl-1 stabilization.

Trametinib triggers the formation of Mcl-1:USP9X complexes in PDAC cells

We noted that USP9X expression levels did not increase in response to trametinib (Figure 4E). Therefore, we investigated

Figure 3. MEK inhibitors stabilize Mcl-1

(A and B) qPCR analysis of *MCL1* mRNA levels in HPNE, PANC 10.05, and CAPAN2 cells following treatment with tram at the indicated concentrations and times. Graphs depict the average change in *MCL1* transcript normalized to UBC and relative to DMSO controls (mean ± SD of technical replicates, n = 3).

(C) Western blots showing levels of Mcl-1 following treatment with 25 nM tram alone or in combination with 5 μM MK2206.

(D) Western blots showing levels of Mcl-1 following treatment with 25 nM tram alone or in combination with 250 nM AZD2014.

(E and F) Levels of Mcl-1 in PANC10.05, CAPAN2, and HPNE cells following treatment with tram for 48 h and the proteasomal inhibitor MG132 (10 μM) for 60 and 120 min prior to lysis.

(G and H) Assessment of Mcl-1 protein stability by cycloheximide (CHX) degradation assays. Western blots show levels of Mcl-1 in PDAC cell lines and HPNE cells treated with DMSO (control) or the indicated concentration of tram for 48 h and treated with CHX for up to 120 min prior to lysis. Graphs depict natural log (ln)-transformed quantification of Mcl-1 normalized to tubulin and relative to non-CHX-treated controls vs. time.

(I) Levels of ubiquitinated Mcl-1 following 25 nM tram treatment for 24 h (CAPAN2) or 48 h (PANC 10.5) with or without 10 μM MG132 2 h prior to lysis, after HA IP, in cells transfected with wild-type HA-tagged ubiquitin (HA-Ub). WCL, whole-cell lysate; IB, immunoblot.

Please cite this article in press as: Perurena et al., USP9X mediates an acute adaptive response to MAPK suppression in pancreatic cancer but creates multiple actionable therapeutic vulnerabilities, Cell Reports Medicine (2023), https://doi.org/10.1016/j.xcrm.2023.101007

CellPress
OPEN ACCESS

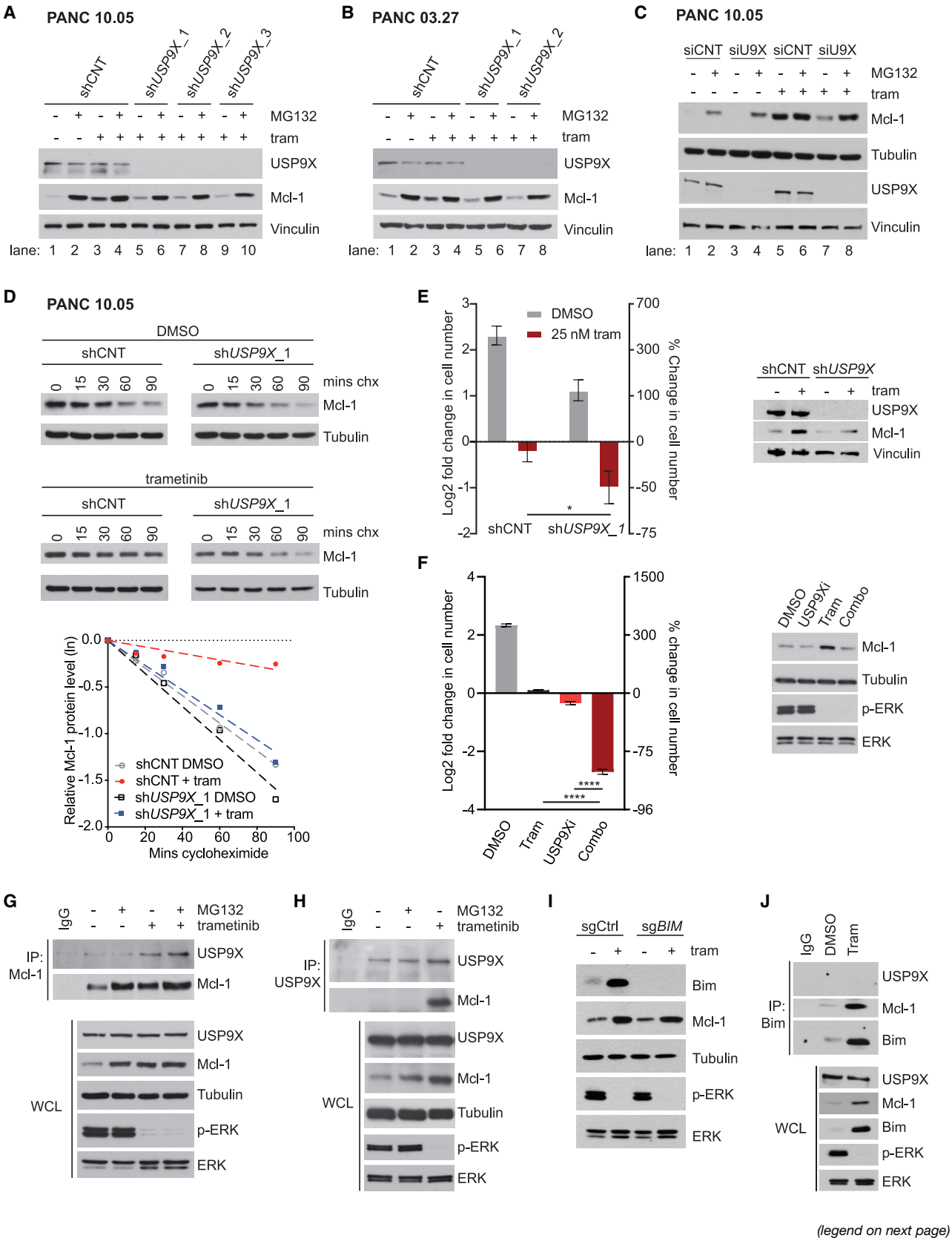

(legend on next page)

Please cite this article in press as: Perurena et al., USP9X mediates an acute adaptive response to MAPK suppression in pancreatic cancer but creates multiple actionable therapeutic vulnerabilities, Cell Reports Medicine (2023), https://doi.org/10.1016/j.xcrm.2023.101007

whether trametinib might be inducing the formation of USP9X:Mcl-1 complexes. Importantly, an increased association between Mcl-1 and USP9X was observed in response to trametinib in the absence and presence of MG132 (Figure 4G). This inducible association was also observed when anti-USP9X antibodies were used to immunoprecipitate the USP9X:Mcl-1 complex (Figure 4H). Notably, an inducible interaction between Mcl-1 and USP9X has not been described previously. Moreover, it was explicitly not observed in 293T cells treated with MEK inhibitors, where USP9X was first identified as the Mcl-1 deubiquitinase.[25] Thus, it appears that this inductive/adaptive mechanism may be specifically important in PDAC and possibly other settings where Mcl-1 is not the dominant anti-apoptotic protein. More importantly however, it suggests that sensitivity to these agents cannot be solely predicted by dependency scores and/or the baseline ratio of anti-apoptotic genes in any given tumor type.

Mcl-1 stabilization is not dependent on Bim

In some settings, Bim has been shown to directly bind and stabilize Mcl-1.[26] Because Bim is upregulated by MEK inhibitors, we investigated whether it might be contributing to the observed stabilization. The Bim gene (*BCL2L11)* was disrupted by stably introducing a CRISPR sgRNA. While Bim expression was effectively eliminated, Mcl-1 was still potently induced by trametinib (Figure 4I). This finding was in stark contrast to the effects of USP9X ablation, which prevented Mcl-1 stabilization (Figures 4A–4D). Of note, we were also unable to detect any USP9X in Bim immunoprecipitates (Figure 4J). Together, these results demonstrate that (1) USP9X plays a dominant role in stabilizing Mcl-1 in PDACs, (2) Bim is not required for Mcl-1 stabilization in this context, and (3) Mcl-1:USP9X and Mcl-1:Bim appear to reside in different complexes. Together they suggest that MEK inhibitors trigger the association between USP9X and Mcl-1, resulting in its deubiquitination and stabilization. When deubiquitinated, deubiquitinase/substrate complexes disassociate, as expected, permitting the formation of Mcl-1:Bim complexes, which block apoptosis.

Mcl-1 inhibitors dramatically sensitize PDAC cells and human tumor organoids to MEK inhibitors

We next examined the effects of trametinib combined with small--molecule Mcl-1 inhibitors. Several Mcl-1 inhibitors have been developed and are in early-stage clinical trials (clinicaltrials.gov; ClinicalTrials.gov: NCT02992483, NCT04629443, NCT02979366, NCT03672695, NCT04837677, NCT05107856, and NCT02675452). The inhibitor S63845 is highly selective for Mcl-1 and exerts single-agent efficacy in Mcl-1 dependent hematologic malignancies.[20] Importantly, while trametinib increased Mcl-1 levels and, consequently, Mcl-1:Bim complexes in PDAC cells, S63845, which directly binds Mcl-1, effectively disrupted this interaction (Figure 5A).

Similar to genetic Mcl-1 depletion experiments, S63845 alone did not induce apoptosis above baseline levels and had no effect on the proliferation of PDAC and HPNE cells (Figures 5B, 5C, and S3A–S3D). However, when combined, S63845 and trametinib dramatically increased apoptosis in PDAC cells (Figure 5B). Consistent with the genetic studies shown in Figures 2D and S1C, the combined suppression of Mcl-1 and MEK resulted in a continued, progressive decrease in cell number over time, as illustrated by longer-term cell counting and crystal violet cell staining assays (Figures 5C, S3A, and S3B). By contrast, trametinib and S63845 did not cooperatively kill HPNE cells or six other non-cancerous human cell lines, as shown by cell counting and/or apoptosis assays, demonstrating that this combination is not generally cytotoxic (pancreatic ductal HPD cells,[27] IMR-90 and BJ fibroblasts, retinal pigment epithelial RPE-1 cells, mammary epithelial MCF10A cells, and adult epidermal keratinocytes HEKa) (Figures S3C and S3D).

These findings suggested that trametinib actively sensitizes PDACs to Mcl-1 inhibitors by increasing Mcl-1 protein levels and, subsequently, Mcl-1:Bim complexes. Therefore, we reasoned that trametinib pre-treatment should prime cells and accelerate cell death in response to the drug combination. To investigate this possibility, PANC 10.05 and PANC 03.27 cells were exposed to trametinib for 48 h and then treated with the S63845/trametinib combination (Figure 5D). Importantly, trametinib pre-treatment resulted in a rapid induction of apoptosis

Figure 4. USP9X mediates Mcl-1 stability following MEK inhibition

(A and B) Western blots depicting levels of Mcl-1 and USP9X in shCNT and sh*USP9X* cells treated with 25 nM tram for 24 h (PANC 10.05) or 48 h (PANC 03.27) with or without 10 μM MG132 2 h prior to lysis.

(C) Western blots depicting levels of Mcl-1 and USP9X in siCNT and siUSP9X (siU9X) PANC 10.05 cells treated with 25 nM tram for 24 h with or without 10 μM MG132 2 h prior to lysis.

(D) Western blots showing levels of Mcl-1 in shCNT and sh*USP9X* PANC 10.05 cells following treatment with 25 nM tram or DMSO (control) for 24 h and treatment with CHX for up to 90 min prior to lysis. The graph depicts ln-transformed quantification of Mcl-1 normalized to tubulin and relative to non-CHX-treated controls.

(E) Graph: log2 fold change (left y axis) and corresponding percent change (right y axis) in cell numbers following infection of PANC 10.05 cells with shCNT or sh*USP9X* and treatment with DMSO or 25 nM tram for 72 h (mean ± SD of technical replicates, n = 3; *$p < 0.05$, unpaired t test). Western blots: levels of Mcl-1 in shCNT and sh*USP9X* PANC 10.05 cells treated with DMSO and 25 nM tram for 24 h.

(F) Graph: log2 fold change (left y axis) and corresponding percent change (right y axis) in cell numbers in PANC 10.05 cells treated with DMSO, 25 nM tram, 3 μM EOAI3402143 (USP9Xi), or the combination (combo) for 72 h (mean ± SD of technical replicates, n = 3; ****$p < 0.0001$, unpaired t test). Western blots: levels of Mcl-1 in PANC 10.05 cells treated with DMSO, 25 nM tram, 3 μM EOAI3402143 (USP9Xi), or combo for 24 h.

(G and H) CoIP of USP9X and Mcl-1 following tram treatment. Mcl-1 (F) or USP9X (G) were immunoprecipitated from PANC 10.05 lysates following treatment with 25 nM tram for 48 h in the presence or absence of 10 μM MG132 to detect USP9X:Mcl-1 complexes.

(I) Western blots of Bim and Mcl-1 levels in PANC 10.05 control (sgCtrl) and *BIM* knockout (sg*BIM*) cells treated with DMSO or 25 nM tram for 24 h.

(J) IP of Bim and western blots of USP9X, Bim, and Mcl-1 in PANC 10.05 cells following treatment with 25 nM tram for 48 h in IP samples and WCLs. See also Figure S2.

Please cite this article in press as: Perurena et al., USP9X mediates an acute adaptive response to MAPK suppression in pancreatic cancer but creates multiple actionable therapeutic vulnerabilities, Cell Reports Medicine (2023), https://doi.org/10.1016/j.xcrm.2023.101007

CellPress
OPEN ACCESS

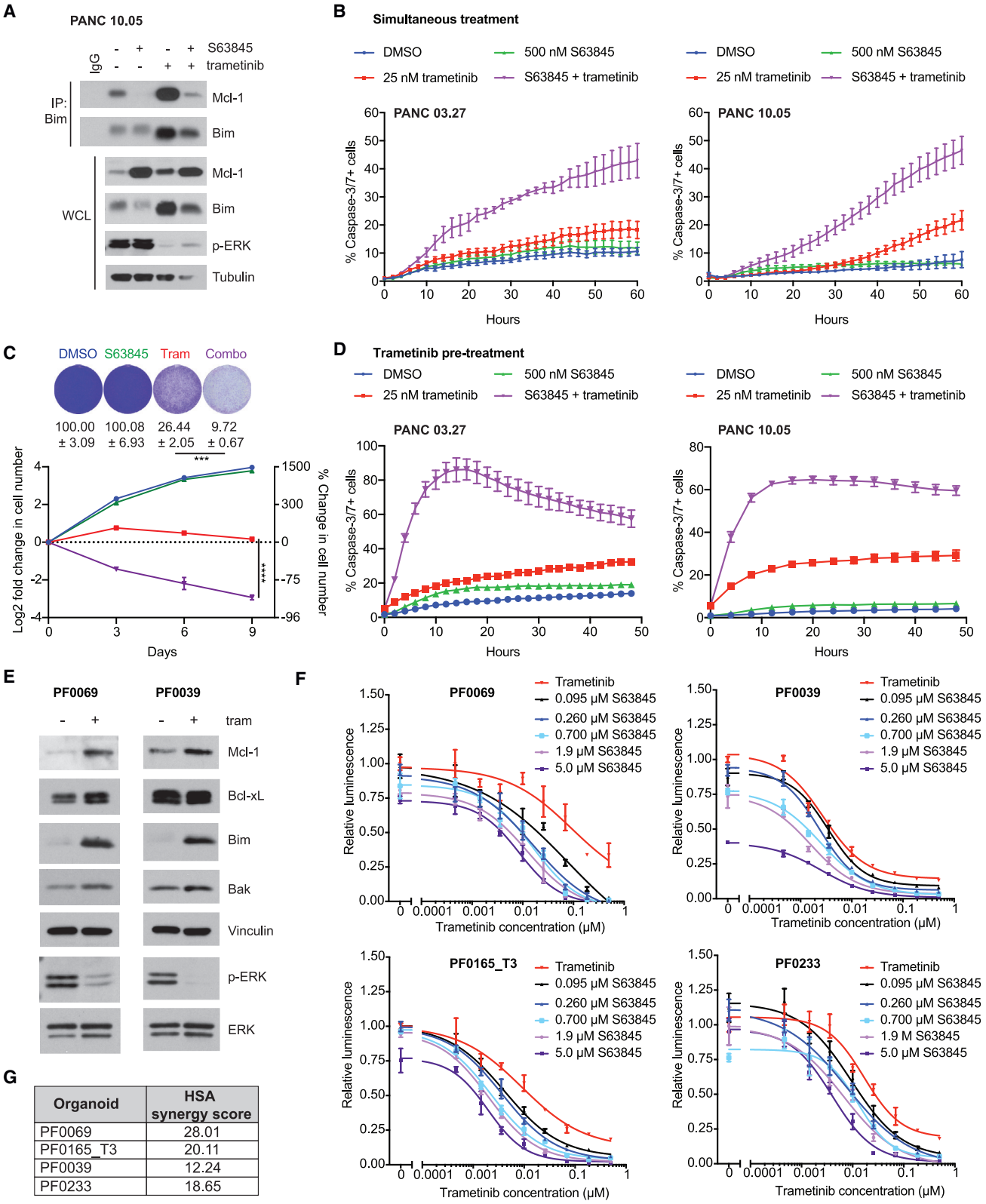

G

Organoid	HSA synergy score
PF0069	28.01
PF0165_T3	20.11
PF0039	12.24
PF0233	18.65

(legend on next page)

Please cite this article in press as: Perurena et al., USP9X mediates an acute adaptive response to MAPK suppression in pancreatic cancer but creates multiple actionable therapeutic vulnerabilities, Cell Reports Medicine (2023), https://doi.org/10.1016/j.xcrm.2023.101007

following combined treatment with S63845 and trametinib, which peaked in approximately 16 h (compare Figures 5B–5D) with a substantial reduction in the time to half-maximal caspase induction (PANC 10.05, 3.8 h vs. 36.3 h; PANC 03.27, 4.1 h vs. 21.6 h; Figure S3E). The efficacy of this combination was further confirmed in two additional PDAC lines, CAPAN2 and HPAC (Figure S3F). Together, these results demonstrate that the dynamic increase in Mcl-1 levels in PDACs plays a critical role in conferring resistance to MEK inhibitors. Considered from a different perspective, these findings also show that, while PDACs are not intrinsically dependent on Mcl-1, MEK inhibition confers a potent Mcl-1 dependency, acutely sensitizing these cells to Mcl-1 inhibitors. It should also be noted that this combination was effective in tumor cells that express one mutant *KRAS* allele (PANC 10.05; Figures 5B, 5D and S3A), in cells with one mutant *KRAS* allele and amplifications in *RAF1* and *MAPK1* (PANC 03.27; Figures 5B–5D), and in those that harbor two mutant alleles[28] (HPAC; Figures 2H and S3F), which are thought to represent a more aggressive subset because of amplification of the RAS signal.[29,30]

We next evaluated S63845 and trametinib in patient-derived PDAC organoids using methods established for therapeutic testing.[31] Importantly, this approach has been shown to be predictive of patient response to chemotherapeutic agents.[31] As observed in PDAC cell lines, trametinib also increased the expression of Mcl-1, Bim, and, to a lesser extent, Bak in these tumor organoids (Figure 5E). Moreover, S63845 potently sensitized four independent PDAC organoid lines to trametinib (Figure 5F). The combined effect of these agents was synergistic as determined by Gaddum's (non-)interaction score (Figure 5G). As observed in PDAC cell lines, these patient-derived organoids were relatively insensitive to S63845 alone (Figure 5F). Together, these findings suggest that combined MEK and Mcl-1 inhibitors may be a viable therapeutic strategy for treating pancreatic cancers, which would not have been predicted by genetic *MCL1* dependency data or by baseline Mcl-1 expression levels.

Transcriptional CDK inhibitors cooperate with trametinib in PDACs by suppressing Mcl-1 transcription

Given that MEK suppression triggered such a strong dependency on Mcl-1, we hypothesized that other agents that suppress Mcl-1 expression, even via other mechanisms, might also cooperate with MEK inhibitors in PDACs. Importantly, transcriptional CDKs, such as CDK9 and, more recently, CDK7 and CDK12, have been shown to critically regulate Mcl-1 transcription by phosphorylating the C-terminal domain (CTD) of RNA polymerase II (RNAPII).[32,33] Accordingly, various CDK inhibitors have been shown to inhibit Mcl-1 expression in AML and other tumor types by suppressing RNAPII phosphorylation, preventing its transcription.[33–35] Therefore, we first investigated the effects of THZ1, a covalent inhibitor of CDK7, CDK12, and CDK13.[34] THZ1 alone potently reduced *MCL1* transcript levels, and suppression was maintained when combined with trametinib (Figure 6A). Accordingly, THZ1 alone progressively reduced baseline Mcl-1 protein expression within 6–24 h, which mirrored the kinetics of RNAPII dephosphorylation (Figure 6B, compare lanes 1, 6, and 9) and suppression of Mcl-1 mRNA (Figure 6A). Moreover, because THZ1 was so effective at suppressing Mcl-1 transcription and, consequently, depleting Mcl-1 transcripts, THZ1 completely prevented the upregulation of Mcl-1 protein triggered by trametinib (Figure 6B, compare lanes 1 and 8 with lane 10). This was expected, given that Mcl-1 mRNA and, consequently, protein were no longer being produced and therefore could not be stabilized. Combined THZ1 and trametinib also potently induced apoptosis (Figure 6C). Notably, these effects were not due to an increase in USP9X expression, which does not change in response to THZ1 (Figure S4A). Similar to trametinib/Mcl-1 inhibitor experiments, combined trametinib and THZ1 triggered a progressive loss of PDAC cells over 7–10 days, as illustrated by crystal violet cell staining (Figure 6D) and cell counting (Figure S4B).

Nevertheless, because THZ1 can affect many transcripts that could potentially contribute to this response, we assessed the requirement for Mcl-1 suppression in mediating cell death in response to trametinib and THZ1. Importantly, ectopic expression of FLAG-HA-MCL1 rescued cell death in response to THZ1 and trametinib, indicating that Mcl-1 suppression is essential for the therapeutic effects of these agents (Figure 6E, right). Of note, THZ1 did not affect the expression of this ectopic construct (Figure 6E, left). Finally, because THZ1 inhibits CDK7, CDK12, and CDK13, we also investigated the therapeutic effects of trametinib and THZ531, which is more selective for

Figure 5. Mcl-1 inhibitors sensitize PDAC cells and patient-derived tumor organoids to MEK inhibitors

(A) IP of Bim:Mcl-1 complexes following treatment with 25 nM tram alone or in combo with 500 nM S63845 for 48 h in PANC 10.05 cells. WCL, whole-cell lysate.

(B) CC3/7 activation kinetics in PANC 10.05 and PANC 03.27 cells following treatment with 25 nM tram, 500 nM S63845, or combo. The graphs depict the average percentage of nuclei that are co-positive for activated CC3/7 (mean ± SEM of 3–4 biological replicates).

(C) Top: crystal violet staining of PANC 03.27 cells treated with DMSO, 500 nM S63845, 50 nM tram or tram + S63845 (combo) for 7 days. One representative image is shown per condition. Numbers indicate absorbance values relative to DMSO (mean ± SD, n = 3; ***$p < 0.001$, unpaired t test). Bottom: graph depicting log2 fold change (left y axis) and percent change (right y axis) in cell numbers in PANC 03.27 cells treated for 9 days with the agents and concentrations indicated above (mean ± SD of technical replicates, n = 3; ****$p < 0.0001$, unpaired t test).

(D) CC3/7 activation kinetics in PANC 10.05 and PANC 03.27 cells following treatment with 25 nM tram, 500 nM S63845, or combo. Cells were pre-treated with tram or DMSO (control) for 48 h before time 0. The graphs depict the average percentage of nuclei that are co-positive for activated CC3/7 (mean ± SEM of 3–4 biological replicates).

(E) Western blots showing changes in the levels of Bcl-2-family proteins in patient-derived organoids following treatment with 50 nM tram for 48 h.

(F) Tram dose-response curves of human-derived organoids treated with tram alone (red) and in combo with the indicated concentrations of S63845 (black, blue, and purple). The graphs depict the average change in luminescence relative to DMSO controls (mean ± SD; DMSO, n = 16; tram and S63845 alone, n = 2; all other combos, n = 3).

(G) Mean Gaddum's non-interaction excess over highest single agent (HSA) synergy scores for each organoid.

See also Figures S3A–S3F.

Please cite this article in press as: Perurena et al., USP9X mediates an acute adaptive response to MAPK suppression in pancreatic cancer but creates multiple actionable therapeutic vulnerabilities, Cell Reports Medicine (2023), https://doi.org/10.1016/j.xcrm.2023.101007

CellPress
OPEN ACCESS

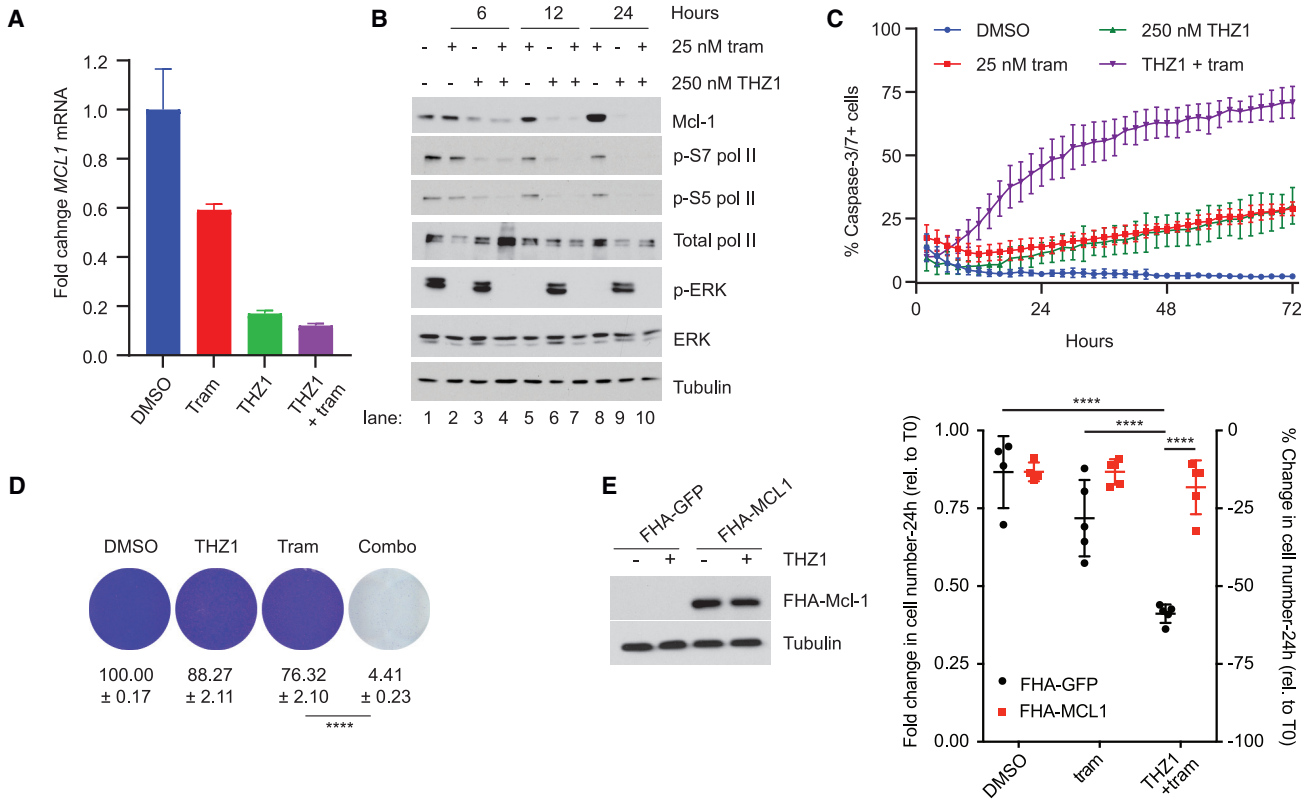

Figure 6. The CDK7/12/13 inhibitor THZ1 cooperates with MEK inhibition to reduce Mcl-1 levels and cause apoptosis

(A) qPCR analysis of *MCL1* mRNA levels in PANC 10.05 cells treated with DMSO, 25 nM tram, 250 nM THZ1, or combo for 24 h. The graph depicts the average change in *MCL1* transcript normalized to UBC and relative to the DMSO control (mean ± SD of technical replicates, n = 3).

(B) Western blots showing levels of Mcl-1 and p-S5 and p-S7 RNAPII in PANC 10.05 cells treated with DMSO, 25 nM tram, 250 nM THZ1, or combo at the indicated time points.

(C) CC3/7 activation kinetics in PANC 10.05 cells treated with 25 nM tram alone or in combo with 250 nM THZ1, pre-treated with tram or DMSO (control) for 48 h before time 0. The graphs depict the average percentage of nuclei that are co-positive for activated CC3/7 (mean ± SD of technical replicates, n = 3).

(D) Crystal violet staining of PANC 03.27 cells treated with DMSO, 100 nM THZ1, 50 nM tram, or THZ1 + tram (combo) for 7 days. One representative image is shown per condition. Numbers indicate absorbance values relative to DMSO (mean ± SD, n = 3; ****p < 0.0001, unpaired t test).

(E) Western blots: exogenous Mcl-1 levels in PANC 10.05 cells expressing FLAG-HA-tagged GFP (FHA-GFP; control) or FHA-MCL1 under DMSO and THZ1-treated conditions. Graph: average fold change (left y axis) and percent change (right y axis) in the number of PANC 10.05 cells expressing FHA-GFP or FHA-MCL1 after 24 h of treatment relative to time 0 (T0). Cells were pre-treated with DMSO or tram for 48 h (mean of biological replicates ± SD; DMSO, n = 4; tram and tram + THZ1, n = 5; ****p < 0.0001, ANOVA followed by Tukey's multiple-comparisons test).

See also Figures S4A–S4D.

CDK12 and CDK13.[36] Interestingly, THZ531 similarly prevented Mcl-1 upregulation in response to MEK inhibition (Figure S4C), and together these agents triggered apoptosis (Figure 4D) and a cooperative loss of cells over time (Figure S4E). These results suggest that the highly related CDK12 and CDK13 are particularly critical for Mcl-1 expression in PDACs and that these agents may represent alternative therapeutic agents that could be used in this context.

Co-suppression of MEK and Mcl-1 via distinct therapeutic strategies induces tumor regression *in vivo*

Finally, we investigated the therapeutic response to these distinct drug combinations *in vivo.* First, the effects of trametinib alone or combined with THZ1 were evaluated in PANC 03.27 and CAPAN2 xenografts. THZ1 treatment alone had a minimal effect on the growth of the majority of tumors in both models (Figures 7A and 7B). Trametinib alone also exerted little effect in PANC 03.27 tumors and cytostatic or modest responses in CAPAN2 tumors (Figures 7A and 7B). However, tumors dramatically regressed in response to the THZ1/trametinib combination. Pharmacodynamic analysis confirmed that MEK inhibitors induced an accumulation of Mcl-1 within 48 h *in vivo*, which was prevented by co-treatment with TZH1 (Figure 7C). Notably, only combined trametinib and THZ1 induced massive cell death, as depicted by wide-spread cell debris and cleaved caspase-3 (CC3) staining in just 3 days (Figure 7D).

Next, we evaluated these agents in a human PDX model from an individual who relapsed after standard chemotherapy (PCA 41). While trametinib or THZ1 each slowed the growth of these tumors, combined THZ1/trametinib treatment was significantly more potent than either agent alone (Figure 7E, left; $p < 0.01$). At first glance, these effects appeared to be cytostatic; however,

Please cite this article in press as: Perurena et al., USP9X mediates an acute adaptive response to MAPK suppression in pancreatic cancer but creates multiple actionable therapeutic vulnerabilities, Cell Reports Medicine (2023), https://doi.org/10.1016/j.xcrm.2023.101007

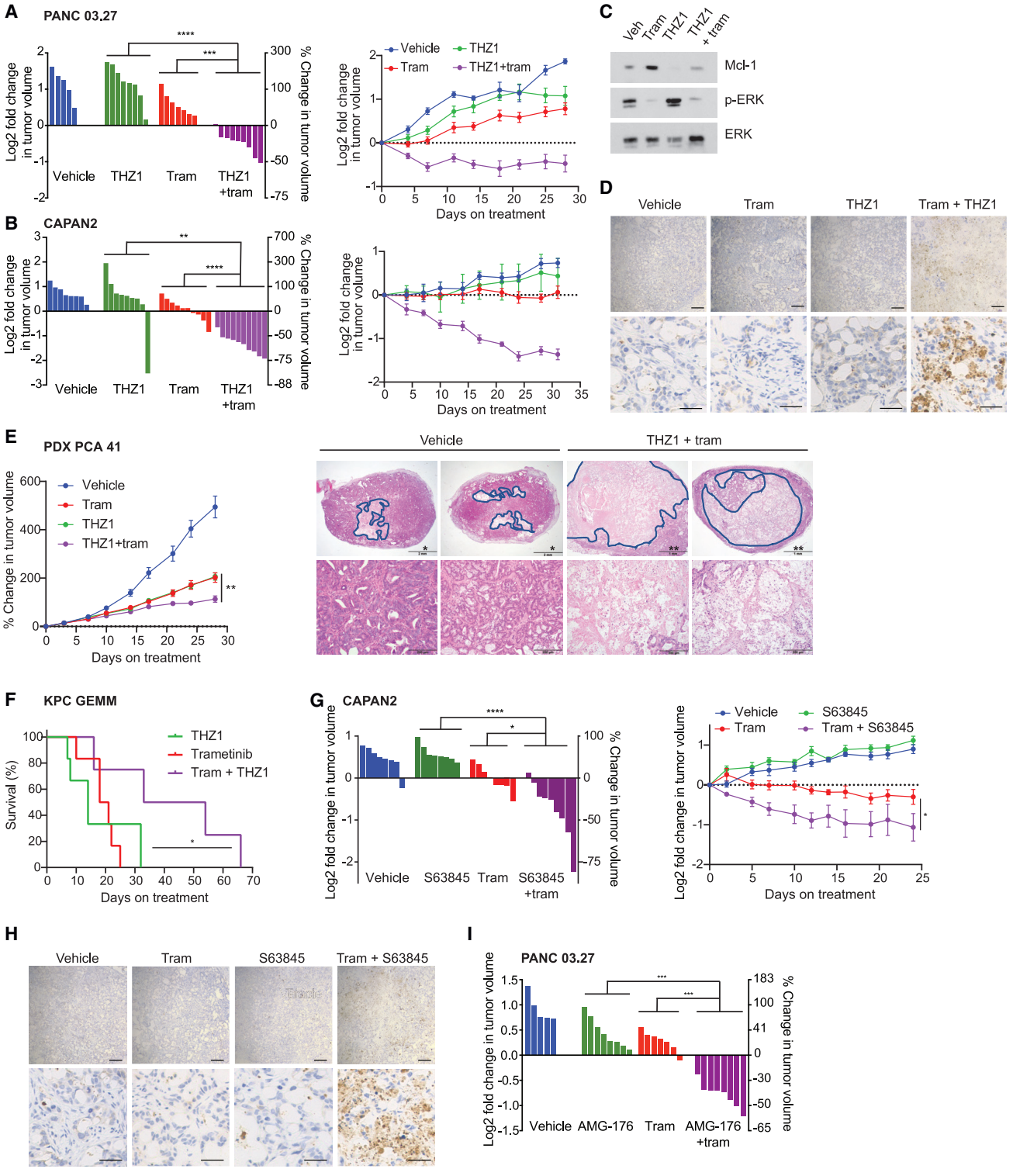

Figure 7. Mcl-1 inhibition cooperates with MEK inhibition *in vivo*

(A and B) Waterfall (left) and tumor volume over time (right) plots depicting the log2 fold change (left y axis) and corresponding percent change (right y axis) in PANC 03.27 and CAPAN2 xenograft models. Waterfall plots indicate tumor volume on days 21 and 31 of treatment (when all animals were still alive), respectively. Each bar represents an individual tumor (PANC 03.27: vehicle, n = 5; THZ1, n = 8; tram, n = 7; combo, n = 9; CAPAN2: vehicle, n = 8; THZ1, n = 9; tram and combo, n = 10; **p < 0.01, ***p < 0.001, ****p < 0.0001, Mann-Whitney test).

(C) Western blots showing Mcl-1 and p-ERK levels in CAPAN2 xenograft tumors after 2 days of treatment.

(legend continued on next page)

Please cite this article in press as: Perurena et al., USP9X mediates an acute adaptive response to MAPK suppression in pancreatic cancer but creates multiple actionable therapeutic vulnerabilities, Cell Reports Medicine (2023), https://doi.org/10.1016/j.xcrm.2023.101007

CellPress
OPEN ACCESS

histological analysis revealed a remarkable loss of the majority of viable cells and extensive cellular debris in combination-treated tumors (Figure 7E, right). These findings suggest that caliper-based tumor volume measurements underestimate the effect of these agents in this model and demonstrate that THZ1 and trametinib also induce massive cell death in human PDX tumors.

Finally, we evaluated the effects of trametinib and THZ1 in a genetically engineered mouse model (GEMM) harboring conditional mutations in *KRAS* and *p53* (Pdx1-Cre; LSL-Kras$^{G12D/+}$; LSL-Trp53$^{R172H/+}$, referred to as the KPC model).[37] Importantly, this model mimics all stages of PDAC development, including metastasis. MEK inhibitors have been shown to be ineffective in this model in multiple studies,[38–40] and we found that THZ1 was similarly ineffective (Figure 7F). Nevertheless, together THZ1 and trametinib significantly prolonged survival in this aggressive model (log rank test, $p = 0.05$).

Direct Mcl-1 inhibitors were also evaluated in the presence and absence of MEK inhibitors *in vivo*. Human xenografts were exclusively used for these studies because Mcl-1 inhibitors do not effectively bind and inhibit mouse Mcl-1 protein.[20,41,42] Notably, we found that S63845 promoted massive tumor regression in CAPAN2 xenografts, but only when combined with trametinib (Figure 7G). A dramatic induction of CC3 within 72 h and a loss of viable cells was further demonstrated by immunohistochemical analysis (Figure 7H). Tumor regression was confirmed using a second structurally distinct Mcl-1 inhibitor, AMG-176, and a second model (PANC 03.27; Figure 7I). However, in this setting, animals were pre-treated with trametinib prior to the addition of AMG-176, suggesting that delayed or perhaps intermittent dosing of Mcl-1 inhibitors may represent a viable strategy. Notably, while all of these drug combinations were well tolerated in mice, potential toxicities in humans could be minimized with this type of approach. Regardless, these studies have identified two distinct therapeutic combinations that effectively kill these deadly malignancies and highlight the importance of deconstructing adaptive pathways to single agents in cancer so that we may develop rational combination therapies.

DISCUSSION

Clinical responses to MEK inhibitors were first observed in *BRAF*-mutant melanomas.[43] Unfortunately, however, clinical trials evaluating MEK inhibitors in *KRAS*-mutant malignancies, including pancreatic cancers, have been largely disappointing.[5,6] Therefore, understanding why these tumors are innately resistant to these agents is essential for developing effective combinatorial therapeutic strategies. Here we describe a critical adaptive response in PDACs that underlies innate resistance to MEK inhibitors. Specifically, we found that MEK inhibitors cause a dramatic upregulation of the anti-apoptotic protein Mcl-1 by acutely enhancing its stability. Mcl-1 can then bind Bim, thus protecting cells from apoptosis. Accordingly, genetic or chemical inhibition of Mcl-1 prevents this protective response and triggers cell death when combined with MEK inhibitors in PDAC cell lines, human tumor organoids, and multiple *in vivo* models. Moreover, we report that direct Mcl-1 inhibitors, as well as CDK inhibitors that block Mcl-1 expression at the level of transcription, cooperate with MEK inhibitors to cause dramatic tumor regression *in vivo*, thus revealing two combinatorial strategies for these currently refractory malignancies. Based on the canonical positive relationship between the RAS pathway and Mcl-1 in normal cells, these findings were unexpected. In fact, this positive regulation of Mcl-1 by the RAS pathway has been coopted for therapeutic benefit in pre-clinical drug combination studies in AML, papillary thyroid cancer, prostate cancer, and colorectal cancer through the use of MEK, RTK, and mTOR inhibitors, which cooperatively reduced Mcl-1 expression in these settings.[16,17,23,44] Nevertheless, in PDACs we observe the opposite response: the Mcl-1 protein is dramatically stabilized by MEK inhibitors.

While MEK- and Bcl-2-family inhibitors have been shown to cooperate in other tumor types, the mechanistic basis for this cooperativity is not known.[20–22] Here we show that the acute increase in Mcl-1 stability is mediated by USP9X, which dynamically associates with Mcl-1 in response to trametinib. USP9X is known to deubiquitinate Mcl-1, but nothing is known about how it may be regulated. In fact, MEK inhibitors have been explicitly reported to have no effect on the Mcl-1:USP9X interaction in HEK293T cells, perhaps because of cell type and/or other experimental differences.[25] We hypothesized that this interaction might be controlled by Mcl-1 phosphorylation, but we did not detect any changes in Mcl-1 at known phosphorylation sites, and gain- and loss-of-function phosphorylation mutants were not informative. Therefore, we speculate that complex formation may be regulated by Mcl-1 phosphorylation/dephosphorylation at (a) unique site(s) or through post-translational modification of USP9X or may be affected by an unknown component, which can be investigated in future studies. Regardless, the findings described here have uncovered a dynamic adaptive mechanism that underlies resistance to Ras pathway suppression in PDACs

(D) CC3 staining in tumor sections after 3 days of treatment. 10× (top) and 20× (bottom) magnification; scale bars, 200 μm and 50 μm, respectively.
(E) Left: percent change in tumor volume over time in a PDX model (PCA 41) treated with vehicle (n = 8), THZ1 (n = 8), tram (n = 7), and combo (n = 8); $^{**}p < 0.01$, Mann-Whitney test. Right: representative H&E images of vehicle- and combo-treated tumors at the conclusion of the study (28 days). Two magnifications are shown for each representative tumor. Scale bars: *2 mm and **1 mm (top), 200 μm (bottom).
(F) Kaplan-Meier survival curves of KPC GEMM mice treated with THZ1 (n = 6), tram (n = 6), and combo (n = 4). THZ1 vs. combo, p = 0.03; tram vs. combo, p = 0.05; log rank test.
(G) Waterfall (left) and tumor volume over time (right) plots depicting the log2 fold change (left y axis) and corresponding percent change (right y axis) in CAPAN2 xenografts treated with vehicle (n = 8), tram (n = 8), SC63845 (n = 8), and combo (n = 9); $p < 0.05$, $^{***}p < 0.001$, Mann-Whitney test.
(H) CC3 staining in tumor sections after 3 days of treatment. 10× (top) and 20× (bottom) magnification; scale bars, 200 μm and 50 μm, respectively.
(I) Waterfall plot depicting the log2 fold change (left y axis) and corresponding percent change (right y axis) in PANC 03.27 xenograft tumor volume on day 10 following treatment with vehicle, AMG-176, tram, or AMG-176 + tram. Mice were treated for 4 days with vehicle (for vehicle and AMG-176 alone) or tram (for tram and AMG-176 + tram), followed by 6 days of treatment with vehicle, AMG-176, tram, or AMG-176 + tram. Each bar represents an individual tumor and vehicle, and tram tumors are day 10 measurements of tumors shown in (A) (vehicle, n = 6; tram, n = 7; AMG-176 and AMG-176 + tram, n = 8; $^{***}p < 0.001$, Mann-Whitney test).

Please cite this article in press as: Perurena et al., USP9X mediates an acute adaptive response to MAPK suppression in pancreatic cancer but creates multiple actionable therapeutic vulnerabilities, Cell Reports Medicine (2023), https://doi.org/10.1016/j.xcrm.2023.101007

and has led to the identification of several therapeutic targets (Mcl-1, USP9X, and CDKs) in this deadly disease.

Several Mcl-1 specific inhibitors have been developed and are in early-stage clinical trials[20,42] (clinicaltrials.gov; ClinicalTrials.gov: NCT02992483, NCT04629443, NCT02979366, NCT03672695, NCT04837677, NCT05107856, and NCT02675452). While these agents are primarily being evaluated in hematopoietic tumors at this time, the observation that Mcl-1 inhibitors are effective when combined with approved MEK inhibitors in multiple pre-clinical models of PDAC makes this finding highly translatable. Recently, a combination comprised of trametinib and chloroquine was shown to exhibit promising activity in PDAC models, which directly led to the development of an ongoing clinical trial.[45] Importantly, like trametinib and chloroquine, all of the drug combinations described in the current study also triggered robust tumor regression and cell death in multiple *in vivo* models. Therefore, these findings have identified two additional promising therapeutic strategies that can be evaluated in clinical trials, which may ultimately improve the current poor prognosis of individuals with PDAC.

Of course, potential toxicities are always of concern, especially in the context of drug combinations. However, using a MEK inhibitor pre-treatment strategy, we have shown that MEK inhibitors sensitize/prime PDAC cells and tumors to Mcl-1 inhibition, resulting in more rapid induction of apoptosis following treatment with S63845. These findings make mechanistic sense because MEK inhibitor pre-treatment results in the accumulation of Mcl-1 protein and Mcl-1:Bim complexes, which are then rapidly freed to initiate apoptosis following exposure to S63845. They also suggest a possible dosing strategy where patients could be treated continuously with MEK inhibitor with intermittent dosing of an Mcl-1 inhibitor, which could limit potential toxicities associated with prolonged combined exposure to Mcl-1 and MEK inhibitors.

Finally, we found that THZ1, a CDK7/12/13 inhibitor, potently cooperates with MEK inhibitors to suppress Mcl-1 expression, trigger apoptosis, and cause tumor regression *in vivo*. While the importance of CDK9 in regulating Mcl-1 transcription in AML has been established,[33] we exploited this insight and here showed that other CDKs, in particular CDK12 and CDK13, are essential for maintaining Mcl-1 expression in PDACs. Importantly, selective CDK12/13 inhibitors have been developed recently,[36] thus providing additional potential therapeutic combinations.

Altogether, these findings uncover a critical adaptive mechanism that underlies the innate resistance of PDACs to MEK inhibitors, resulting in an inducible therapeutic dependency, and have revealed distinct combinatorial strategies that can be used to overcome resistance and drive tumor regression.

Limitations of the study

In this study, we show that the Mcl-1 protein is stabilized in response to MEK inhibition, but when combined, MEK and Mcl-1 inhibitors kill 4 pancreatic cell lines and 4 pancreatic organoids and induce the regression of xenografts *in vivo*. In addition, combined MEK and CDK inhibitors are similarly effective *in vitro* and in additional models *in vivo* (xenografts, a human PDX, and the KPC GEMM). However, it is possible that not all pancreatic cancers will be sensitive to this combination and that expanding the study to additional models could reveal a subset where Mcl-1 upregulation does not mediate survival and/or does not occur. Indeed, additional experiments are required to elucidate the precise molecular mechanism by which MEK inhibition triggers the association between Mcl-1 and USP9X and to understand why this occurs in pancreatic cancer. In addition, while our studies identify USP9X as a potential therapeutic target in PDAC, the development of more specific USP9X inhibitors is warranted. Finally, while we have shown that combined MEK/Mcl-1 and MEK/CDK7, CDK12, and CDK13 inhibition is not toxic in mice, the tolerability of these therapeutic strategies in humans can only be evaluated in clinical trials.

STAR★METHODS

Detailed methods are provided in the online version of this paper and include the following:

- KEY RESOURCES TABLE
- RESOURCE AVAILABILITY
  - Lead contact
  - Materials availability
  - Data and code availability
- EXPERIMENTAL MODEL AND SUBJECT DETAILS
  - Human specimens
  - Animals
  - Cell lines
- METHOD DETAILS
  - Drugs
  - Incucyte analysis of caspase activation and cell counts
  - Cell counting data
  - Crystal violet staining assays
  - *In vitro* pre-treatment experiments
  - Transfections and infections
  - RNA extraction and quantitative PCR
  - Western blotting
  - Cycloheximide degradation assay
  - Immunoprecipitation of Mcl-1 and Bim to detect complexes
  - Immunoprecipitation of Mcl-1 and USP9X for Mcl-1:USP9X interaction
  - Mcl-1 ubiquitination assay
  - Initiation and culture of human patient-derived pancreatic cancer organoid models
  - Patient-derived organoid compound testing and western blotting
  - Cell line-derived xenografts
  - Human PDX model
  - KPC GEMM experiment
  - *In vivo* drug treatments
  - Immunohistochemistry
- QUANTIFICATION AND STATISTICAL ANALYSIS

SUPPLEMENTAL INFORMATION

Supplemental information can be found online at https://doi.org/10.1016/j.xcrm.2023.101007.

Please cite this article in press as: Perurena et al., USP9X mediates an acute adaptive response to MAPK suppression in pancreatic cancer but creates multiple actionable therapeutic vulnerabilities, Cell Reports Medicine (2023), https://doi.org/10.1016/j.xcrm.2023.101007

ACKNOWLEDGMENTS

This work was supported by grants from the NCI R01 CA111754 (K.C.) and U01 CA176058 (W.C.H.); the Lustgarten Foundation (B.M.W.); the Hale Center for Pancreatic Cancer (B.M.W., N.G., and A.J.A.); Cancer Research UK Beatson Institute awards A17196 (O.J.S.), A29996 (J.P.M.), and A25233 (J.P.M.); and a Hope Funds for Cancer Research Postdoctoral Fellowship (S.R.). The graphical abstract was created using BioRender.

AUTHOR CONTRIBUTIONS

K.C., N.P., and R.L. conceived the project and wrote the manuscript. N.P., R.L., R.A.D., S.R., N.F.P., R.N., P.L., C.J.G., A.L.M., and E.S. performed all experiments. S.S. performed the pathology on PDX tumors. J.P.M. and O.J.S. were critical for the GEMM experiment. J.M.C., D.A.R., and B.M.W. were integral in recruiting patients and establishing tumor organoids. A.J.A., B.M.W., N.S.G., and W.C.H. were critical in designing experiments and editing the manuscript.

DECLARATION OF INTERESTS

K.C. is an advisor at Genentech and serves on the scientific advisory board of Erasca, Inc. N.S.G. is a founder, science advisory board (SAB) member, and equity holder in Gatekeeper, Syros, Petra, C4, B2S, Aduro, Inception, Allorion, Jengu, Larkspur (board member), and Soltego (board member). The Gray lab receives or has received research funding from Novartis, Takeda, Astellas, Taiho, Janssen, Kinogen, Voronoi, Arbella, Deerfield, and Sanofi. A.J.A. has consulted for Oncorus, Inc.; Arrakis Therapeutics; Syros Pharmaceuticals; Boehringer Ingelheim; T-knife Therapeutics; AstraZeneca; and Merck & Co., Inc. and has research funding from Mirati Therapeutics; Syros Pharmaceuticals; Bristol Myers Squibb; Revolution Medicines; Novartis; Deerfield, Inc.; and Novo Ventures that is unrelated to this work. W.C.H. is a consultant for Thermo Fisher, Calyx, Solasta Ventures, MPM, KSQ Therapeutics, Tyra Biosciences, RAPPTA Therapeutics, Function Oncology, Jubilant Therapeutics, and Frontier Medicines. B.M.W. declares research funding from Celgene Inc. and Eli Lilly and Company and consulting for BioLineRx Ltd., Celgene Inc., and GRAIL Inc. O.J.S. receives funding from AstraZeneca, Novartis, Boehringer Ingelheim, Redex, and Cancer Research Technologies. S.S. is a consultant for RareCyte Inc. S.R. holds equity in Amgen.

Received: May 17, 2022
Revised: July 18, 2022
Accepted: March 17, 2023
Published: April 7, 2023

REFERENCES

1. Siegel, R.L., Miller, K.D., and Jemal, A. (2016). Cancer statistics, 2016. CA. Cancer J. Clin. *66*, 7–30. https://doi.org/10.3322/caac.21332.
2. Rubinson, D.A., and Wolpin, B.M. (2015). Therapeutic approaches for metastatic pancreatic adenocarcinoma. Hematol. Oncol. Clin. North Am. *29*, 761–776. https://doi.org/10.1016/j.hoc.2015.04.012.
3. Li, S., Balmain, A., and Counter, C.M. (2018). A model for RAS mutation patterns in cancers: finding the sweet spot. Nat. Rev. Cancer *18*, 767–777. https://doi.org/10.1038/s41568-018-0076-6.
4. Hofmann, M.H., Gerlach, D., Misale, S., Petronczki, M., and Kraut, N. (2022). Expanding the reach of precision Oncology by drugging all KRAS mutants. Cancer Discov. *12*, 924–937. https://doi.org/10.1158/2159-8290.Cd-21-1331.
5. Hymowitz, S.G., and Malek, S. (2018). Targeting the MAPK pathway in RAS mutant cancers. Cold Spring Harb. Perspect. Med. *8*, a031492. https://doi.org/10.1101/cshperspect.a031492.
6. Infante, J.R., Somer, B.G., Park, J.O., Li, C.P., Scheulen, M.E., Kasubhai, S.M., Oh, D.Y., Liu, Y., Redhu, S., Steplewski, K., and Le, N. (2014). A randomised, double-blind, placebo-controlled trial of trametinib, an oral MEK inhibitor, in combination with gemcitabine for patients with untreated metastatic adenocarcinoma of the pancreas. Eur. J. Cancer *50*, 2072–2081. https://doi.org/10.1016/j.ejca.2014.04.024.
7. Reginato, M.J., Mills, K.R., Paulus, J.K., Lynch, D.K., Sgroi, D.C., Debnath, J., Muthuswamy, S.K., and Brugge, J.S. (2003). Integrins and EGFR coordinately regulate the pro-apoptotic protein Bim to prevent anoikis. Nat. Cell Biol. *5*, 733–740. https://doi.org/10.1038/ncb1026.
8. Juin, P., Geneste, O., Gautier, F., Depil, S., and Campone, M. (2013). Decoding and unlocking the BCL-2 dependency of cancer cells. Nat. Rev. Cancer *13*, 455–465. https://doi.org/10.1038/nrc3538.
9. Meng, J., Fang, B., Liao, Y., Chresta, C.M., Smith, P.D., and Roth, J.A. (2010). Apoptosis induction by MEK inhibition in human lung cancer cells is mediated by Bim. PLoS One *5*, e13026. https://doi.org/10.1371/journal.pone.0013026.
10. Townsend, K.J., Zhou, P., Qian, L., Bieszczad, C.K., Lowrey, C.H., Yen, A., and Craig, R.W. (1999). Regulation of MCL1 through a serum response factor/Elk-1-mediated mechanism links expression of a viability-promoting member of the BCL2 family to the induction of hematopoietic cell differentiation. J. Biol. Chem. *274*, 1801–1813.
11. Boros, J., Donaldson, I.J., O'Donnell, A., Odrowaz, Z.A., Zeef, L., Lupien, M., Meyer, C.A., Liu, X.S., Brown, M., and Sharrocks, A.D. (2009). Elucidation of the ELK1 target gene network reveals a role in the coordinate regulation of core components of the gene regulation machinery. Genome Res. *19*, 1963–1973. https://doi.org/10.1101/gr.093047.109.
12. Ding, Q., Huo, L., Yang, J.Y., Xia, W., Wei, Y., Liao, Y., Chang, C.J., Yang, Y., Lai, C.C., Lee, D.F., et al. (2008). Down-regulation of myeloid cell leukemia-1 through inhibiting Erk/Pin 1 pathway by sorafenib facilitates chemosensitization in breast cancer. Cancer Res. *68*, 6109–6117. https://doi.org/10.1158/0008-5472.Can-08-0579.
13. Domina, A.M., Vrana, J.A., Gregory, M.A., Hann, S.R., and Craig, R.W. (2004). MCL1 is phosphorylated in the PEST region and stabilized upon ERK activation in viable cells, and at additional sites with cytotoxic okadaic acid or taxol. Oncogene *23*, 5301–5315. https://doi.org/10.1038/sj.onc.1207692.
14. Bolomsky, A., Vogler, M., Köse, M.C., Heckman, C.A., Ehx, G., Ludwig, H., and Caers, J. (2020). MCL-1 inhibitors, fast-lane development of a new class of anti-cancer agents. J. Hematol. Oncol. *13*, 173. https://doi.org/10.1186/s13045-020-01007-9.
15. Warr, M.R., and Shore, G.C. (2008). Unique biology of Mcl-1: therapeutic opportunities in cancer. Curr. Mol. Med. *8*, 138–147.
16. Gunda, V., Sarosiek, K.A., Brauner, E., Kim, Y.S., Amin, S., Zhou, Z., Letai, A., and Parangi, S. (2017). Inhibition of MAPKinase pathway sensitizes thyroid cancer cells to ABT-737 induced apoptosis. Cancer Lett. *395*, 1–10. https://doi.org/10.1016/j.canlet.2017.02.028.
17. Pan, R., Ruvolo, V., Mu, H., Leverson, J.D., Nichols, G., Reed, J.C., Konopleva, M., and Andreeff, M. (2017). Synthetic lethality of combined Bcl-2 inhibition and p53 activation in AML: mechanisms and superior antileukemic efficacy. Cancer Cell *32*, 748–760.e6. https://doi.org/10.1016/j.ccell.2017.11.003.
18. Kawakami, H., Huang, S., Pal, K., Dutta, S.K., Mukhopadhyay, D., and Sinicrope, F.A. (2016). Mutant BRAF upregulates MCL-1 to confer apoptosis resistance that is reversed by MCL-1 antagonism and cobimetinib in colorectal cancer. Mol. Cancer Ther. *15*, 3015–3027. https://doi.org/10.1158/1535-7163.Mct-16-0017.
19. Elgendy, M., Abdel-Aziz, A.K., Renne, S.L., Bornaghi, V., Procopio, G., Colecchia, M., Kanesvaran, R., Toh, C.K., Bossi, D., Pallavicini, I., et al. (2017). Dual modulation of MCL-1 and mTOR determines the response to sunitinib. J. Clin. Invest. *127*, 153–168. https://doi.org/10.1172/jci84386.
20. Kotschy, A., Szlavik, Z., Murray, J., Davidson, J., Maragno, A.L., Le Toumelin-Braizat, G., Chanrion, M., Kelly, G.L., Gong, J.N., Moujalled, D.M., et al. (2016). The MCL1 inhibitor S63845 is tolerable and effective in diverse cancer models. Nature *538*, 477–482. https://doi.org/10.1038/nature19830.

Please cite this article in press as: Perurena et al., USP9X mediates an acute adaptive response to MAPK suppression in pancreatic cancer but creates multiple actionable therapeutic vulnerabilities, Cell Reports Medicine (2023), https://doi.org/10.1016/j.xcrm.2023.101007

21. Corcoran, R.B., Cheng, K.A., Hata, A.N., Faber, A.C., Ebi, H., Coffee, E.M., Greninger, P., Brown, R.D., Godfrey, J.T., Cohoon, T.J., et al. (2013). Synthetic lethal interaction of combined BCL-XL and MEK inhibition promotes tumor regressions in KRAS mutant cancer models. Cancer Cell *23*, 121–128. https://doi.org/10.1016/j.ccr.2012.11.007.

22. Nangia, V., Siddiqui, F.M., Caenepeel, S., Timonina, D., Bilton, S.J., Phan, N., Gomez-Caraballo, M., Archibald, H.L., Li, C., Fraser, C., et al. (2018). Exploiting MCL1 dependency with combination MEK + MCL1 inhibitors leads to induction of apoptosis and tumor regression in KRAS-mutant non-small cell lung cancer. Cancer Discov. *8*, 1598–1613. https://doi.org/10.1158/2159-8290.Cd-18-0277.

23. Faber, A.C., Coffee, E.M., Costa, C., Dastur, A., Ebi, H., Hata, A.N., Yeo, A.T., Edelman, E.J., Song, Y., Tam, A.T., et al. (2014). mTOR inhibition specifically sensitizes colorectal cancers with KRAS or BRAF mutations to BCL-2/BCL-XL inhibition by suppressing MCL-1. Cancer Discov. *4*, 42–52. https://doi.org/10.1158/2159-8290.CD-13-0315.

24. Mojsa, B., Lassot, I., and Desagher, S. (2014). Mcl-1 ubiquitination: unique regulation of an essential survival protein. Cells *3*, 418–437. https://doi.org/10.3390/cells3020418.

25. Schwickart, M., Huang, X., Lill, J.R., Liu, J., Ferrando, R., French, D.M., Maecker, H., O'Rourke, K., Bazan, F., Eastham-Anderson, J., et al. (2010). Deubiquitinase USP9X stabilizes MCL1 and promotes tumour cell survival. Nature *463*, 103–107. https://doi.org/10.1038/nature08646.

26. Conage-Pough, J.E., and Boise, L.H. (2018). Phosphorylation alters Bim-mediated Mcl-1 stabilization and priming. FEBS J. *285*, 2626–2640. https://doi.org/10.1111/febs.14505.

27. Furukawa, T., Duguid, W.P., Rosenberg, L., Viallet, J., Galloway, D.A., and Tsao, M.S. (1996). Long-term culture and immortalization of epithelial cells from normal adult human pancreatic ducts transfected by the E6E7 gene of human papilloma virus 16. Am. J. Pathol. *148*, 1763–1770.

28. Tew, B.Y., Durand, J.K., Bryant, K.L., Hayes, T.K., Peng, S., Tran, N.L., Gooden, G.C., Buckley, D.N., Der, C.J., Baldwin, A.S., and Salhia, B. (2020). Genome-wide DNA methylation analysis of KRAS mutant cell lines. Sci. Rep. *10*, 10149. https://doi.org/10.1038/s41598-020-66797-x.

29. Hayashi, A., Hong, J., and Iacobuzio-Donahue, C.A. (2021). The pancreatic cancer genome revisited. Nat. Rev. Gastroenterol. Hepatol. *18*, 469–481. https://doi.org/10.1038/s41575-021-00463-z.

30. Connor, A.A., and Gallinger, S. (2022). Pancreatic cancer evolution and heterogeneity: integrating omics and clinical data. Nat. Rev. Cancer *22*, 131–142. https://doi.org/10.1038/s41568-021-00418-1.

31. Tiriac, H., Belleau, P., Engle, D.D., Plenker, D., Deschênes, A., Somerville, T.D.D., Froeling, F.E.M., Burkhart, R.A., Denroche, R.E., Jang, G.H., et al. (2018). Organoid profiling identifies common responders to chemotherapy in pancreatic cancer. Cancer Discov. *8*, 1112–1129. https://doi.org/10.1158/2159-8290.Cd-18-0349.

32. Jeronimo, C., Collin, P., and Robert, F. (2016). The RNA polymerase II CTD: the increasing complexity of a low-complexity protein domain. J. Mol. Biol. *428*, 2607–2622. https://doi.org/10.1016/j.jmb.2016.02.006.

33. Boffo, S., Damato, A., Alfano, L., and Giordano, A. (2018). CDK9 inhibitors in acute myeloid leukemia. J. Exp. Clin. Cancer Res. *37*, 36. https://doi.org/10.1186/s13046-018-0704-8.

34. Kwiatkowski, N., Zhang, T., Rahl, P.B., Abraham, B.J., Reddy, J., Ficarro, S.B., Dastur, A., Amzallag, A., Ramaswamy, S., Tesar, B., et al. (2014). Targeting transcription regulation in cancer with a covalent CDK7 inhibitor. Nature *511*, 616–620. https://doi.org/10.1038/nature13393.

35. Zeng, M., Kwiatkowski, N.P., Zhang, T., Nabet, B., Xu, M., Liang, Y., Quan, C., Wang, J., Hao, M., Palakurthi, S., et al. (2018). Targeting MYC dependency in ovarian cancer through inhibition of CDK7 and CDK12/13. Elife *7*, e39030. https://doi.org/10.7554/eLife.39030.

36. Zhang, T., Kwiatkowski, N., Olson, C.M., Dixon-Clarke, S.E., Abraham, B.J., Greifenberg, A.K., Ficarro, S.B., Elkins, J.M., Liang, Y., Hannett, N.M., et al. (2016). Covalent targeting of remote cysteine residues to develop CDK12 and CDK13 inhibitors. Nat. Chem. Biol. *12*, 876–884. https://doi.org/10.7554/eLife.3903010.1038/nchembio.2166.

37. Hingorani, S.R., Wang, L., Multani, A.S., Combs, C., Deramaudt, T.B., Hruban, R.H., Rustgi, A.K., Chang, S., and Tuveson, D.A. (2005). Trp53R172H and KrasG12D cooperate to promote chromosomal instability and widely metastatic pancreatic ductal adenocarcinoma in mice. Cancer Cell *7*, 469–483. https://doi.org/10.1016/j.ccr.2005.04.023.

38. Ponz-Sarvise, M., Corbo, V., Tiriac, H., Engle, D.D., Frese, K.K., Oni, T.E., Hwang, C.I., Öhlund, D., Chio, I.I.C., Baker, L.A., et al. (2019). Identification of resistance pathways specific to malignancy using organoid models of pancreatic cancer. Clin. Cancer Res. *25*, 6742–6755. https://doi.org/10.1158/1078-0432.Ccr-19-1398.

39. Grbovic-Huezo, O., Pitter, K.L., Lecomte, N., Saglimbeni, J., Askan, G., Holm, M., Melchor, J.P., Chandwani, R., Joshi, S., Haglund, C., et al. (2020). Unbiased in vivo preclinical evaluation of anticancer drugs identifies effective therapy for the treatment of pancreatic adenocarcinoma. Proc. Natl. Acad. Sci. USA *117*, 30670–30678. https://doi.org/10.1073/pnas.1920240117.

40. Ruscetti, M., Leibold, J., Bott, M.J., Fennell, M., Kulick, A., Salgado, N.R., Chen, C.C., Ho, Y.J., Sanchez-Rivera, F.J., Feucht, J., et al. (2018). NK cell-mediated cytotoxicity contributes to tumor control by a cytostatic drug combination. Science *362*, 1416–1422. https://doi.org/10.1126/science.aas9090.

41. Tron, A.E., Belmonte, M.A., Adam, A., Aquila, B.M., Boise, L.H., Chiarparin, E., Cidado, J., Embrey, K.J., Gangl, E., Gibbons, F.D., et al. (2018). Discovery of Mcl-1-specific inhibitor AZD5991 and preclinical activity in multiple myeloma and acute myeloid leukemia. Nat. Commun. *9*, 5341. https://doi.org/10.1038/s41467-018-07551-w.

42. Caenepeel, S., Brown, S.P., Belmontes, B., Moody, G., Keegan, K.S., Chui, D., Whittington, D.A., Huang, X., Poppe, L., Cheng, A.C., et al. (2018). AMG 176, a selective MCL1 inhibitor, is effective in hematologic cancer models alone and in combination with established therapies. Cancer Discov. *8*, 1582–1597. https://doi.org/10.1158/2159-8290.Cd-18-0387.

43. Flaherty, K.T., Robert, C., Hersey, P., Nathan, P., Garbe, C., Milhem, M., Demidov, L.V., Hassel, J.C., Rutkowski, P., Mohr, P., et al. (2012). Improved survival with MEK inhibition in BRAF-mutated melanoma. N. Engl. J. Med. *367*, 107–114. https://doi.org/10.1056/NEJMoa1203421.

44. Arai, S., Jonas, O., Whitman, M.A., Corey, E., Balk, S.P., and Chen, S. (2018). Tyrosine kinase inhibitors increase MCL1 degradation and in combination with BCLXL/BCL2 inhibitors drive prostate cancer apoptosis. Clin. Cancer Res. *24*, 5458–5470. https://doi.org/10.1158/1078-0432.Ccr-18-0549.

45. Kinsey, C.G., Camolotto, S.A., Boespflug, A.M., Guillen, K.P., Foth, M., Truong, A., Schuman, S.S., Shea, J.E., Seipp, M.T., Yap, J.T., et al. (2019). Protective autophagy elicited by RAF→MEK→ERK inhibition suggests a treatment strategy for RAS-driven cancers. Nat. Med. *25*, 620–627. https://doi.org/10.1038/s41591-019-0367-9.

46. Boj, S.F., Hwang, C.I., Baker, L.A., Engle, D.D., Tuveson, D.A., and Clevers, H. (2016). Model organoids provide new research opportunities for ductal pancreatic cancer. Mol. Cell. Oncol. *3*, e1014757. https://doi.org/10.1080/23723556.2015.1014757.

47. Raghavan, S., Winter, P.S., Navia, A.W., Williams, H.L., DenAdel, A., Lowder, K.E., Galvez-Reyes, J., Kalekar, R.L., Mulugeta, N., Kapner, K.S., et al. (2021). Microenvironment drives cell state, plasticity, and drug response in pancreatic cancer. Cell *184*, 6119–6137.e26. https://doi.org/10.1016/j.cell.2021.11.017.

Please cite this article in press as: Perurena et al., USP9X mediates an acute adaptive response to MAPK suppression in pancreatic cancer but creates multiple actionable therapeutic vulnerabilities, Cell Reports Medicine (2023), https://doi.org/10.1016/j.xcrm.2023.101007

CellPress
OPEN ACCESS

STAR★METHODS

KEY RESOURCES TABLE

REAGENT or RESOURCE	SOURCE	IDENTIFIER
Antibodies		
Anti-Mcl-1	Cell Signaling Technology	Cat#5453; RRID: AB_10694494
Anti-Mcl-1	Cell Signaling Technology	Cat#94296; RRID: AB_2722740
Anti-Mcl-1	Santa Cruz Biotechnology	Cat#sc-819; RRID: AB_2144105
Anti-Mcl-1	Santa Cruz Biotechnology	Cat#sc-12756; RRID: AB_627915
Anti-Mcl-1	Abcam	Cat#ab32087; RRID: AB_776245
Anti-Bcl-xL	Cell Signaling Technology	Cat#2762; RRID: AB_10694844
Anti-Bcl-xL	Cell Signaling Technology	Cat#2764; RRID: AB_2228008
Anti-BIM	Cell Signaling Technology	Cat#2819; RRID: AB_10692515
Anti-Bcl-2	Cell Signaling Technology	Cat#2872; RRID: AB_10693462
Anti-Bak	Cell Signaling Technology	Cat#12105; RRID: AB_2716685
Anti-Bax	Cell Signaling Technology	Cat#2772; RRID: AB_10695870
Anti-phospho-ERK	Cell Signaling Technology	Cat#4370; RRID: AB_2315112
Anti-ERK	Cell Signaling Technology	Cat#9102; RRID: AB_330744
Anti-vinculin	Cell Signaling Technology	Cat#4650; RRID: AB_10559207
Anti-phospho-AKT	Cell Signaling Technology	Cat#4060; RRID: AB_2315049
Anti-AKT	Cell Signaling Technology	Cat#9272; RRID: AB_329827
Anti-phospho-S6 ribosomal protein	Cell Signaling Technology	Cat#2215; RRID: AB_331682
Anti-S6 ribosomal protein	Cell Signaling Technology	Cat#2217; RRID: AB_331355
Anti-phospho-p70 S6 kinase	Cell Signaling Technology	Cat#9205; RRID: AB_330944
Anti-p70 S6 kinase	Cell Signaling Technology	Cat#9202; RRID: AB_331676
Anti-USP9X	Cell Signaling Technology	Cat#14898; RRID: AB_2798640
Anti-USP9X	Abnova	Cat#H00008339-M01; RRID: AB_549092
Anti-phospho-S2 CTD Pol II	EMD Millipore	Cat#04–1571; RRID: AB_10627998
Anti-phospho-S5 CTD Pol II	EMD Millipore	Cat#04–1572; RRID: AB_10615822
Anti-phospho-S7 CTD Pol II	EMD Millipore	Cat#04–1570; RRID: AB_10618152
Anti-RNA Pol II	Abcam	Cat#ab817; RRID: AB_306327
Anti-alpha-tubulin	Sigma-Aldrich	Cat#T5168; RRID: AB_477579
Normal rabbit IgG	EMD Millipore	Cat#12–370: RRID: AB_145841
Normal mouse IgG	EMD Millipore	Cat#12–371: RRID: AB_145840
Anti-cleaved caspase 3	Cell Signaling Technology	Cat#9664; RRID: AB_2070042
Bacterial and virus strains		
cDNA, shRNA and sgRNA constructs were packed into VSV-G typed lentiviral particles in 293T cells using second generation packaging constructs	N/A	N/A
Incucyte Nuclight Red Lentivirus (EF1a, Puro)	Sartorius	Cat#4625
Biological samples		
PCA 41; human PDAC	DFCI	N/A
Chemicals, peptides, and recombinant proteins		
GSK1120212 (Trametinib, MEKi) for *in vitro*	Selleck Chemicals	Cat#S2673; CAS#871700-17-3
GSK1120212 (Trametinib, MEKi) for *in vivo*	LC Laboratories	Cat#T-8123; CAS#871700-17-3
MK2206 (AKTi)	Selleck Chemicals	Cat#S1078; CAS#1032350-13-2
AZD2014 (mTORi)	Selleck Chemicals	Cat#S2783; CAS#1009298-59-2
S63845 (Mcl-1i)	ChemieTek	Cat#CT-S63845; CAS#1799633-27-4

(*Continued on next page*)

Please cite this article in press as: Perurena et al., USP9X mediates an acute adaptive response to MAPK suppression in pancreatic cancer but creates multiple actionable therapeutic vulnerabilities, Cell Reports Medicine (2023), https://doi.org/10.1016/j.xcrm.2023.101007

Continued

REAGENT or RESOURCE	SOURCE	IDENTIFIER
AMG-176 (Mcl-1i)	ChemieTek	Cat#CT-AMG176; CAS#1883727-34-1
EOAI3402143 (USP9Xi)	Selleck Chemicals	Cat#S6877; CAS#1699750-95-2
MG132	Millipore Sigma	Cat#474790; CAS#133407-82-6
Cycloheximide	Sigma-Aldrich	Cat#C7698; CAS#66-81-9
THZ1	MedChem Express	Cat#HY-80013; CAS#1604810-83-4
THZ531	Gift from Nathanael Gray	N/A
Staurosporine	Sigma-Aldrich	Cat#S5921; CAS#62996-74-1
Etoposide	Sigma-Aldrich	Cat#341205; CAS#33419-42-0
Critical commercial assays		
Incucyte Nuclight Rapid Red Dye	Sartorius	Cat#4717
Cell Event Caspase-3/7 Green Detection Reagent	Invitrogen	Cat#C10423
CellTiter-Glo 3D Cell Viability Assay	Promega	Cat#PRG9681
Lipofectamine RNAiMAX Transfection Reagent	Invitrogen	Cat#13778150
x-TremeGENE 9 DNA Transfection Reagent	Roche	Cat#6365787001
RNeasy Plus Mini Kit	Qiagen	Cat#74136
qScript cDNA synthesis Kit	QuantaBio	Cat#95047-500
PerfeCTa SYBR Green Super-Mix Reagent	QuantaBio	Cat#95054-500
cOmplete Mini EDTA-free Protease Inhibitor Cocktail	Roche	Cat#11836170001
PhosSTOP phosphatase inhibitor tables	Roche	Cat#4906837001
BCA Protein Assay Kit	Pierce	Cat#23225
Anti-HA magnetic beads	Pierce	Cat#88836
Protein A magnetic beads	Pierce	Cat#88846
Protein G magnetic beads	Pierce	Cat#88847
Experimental models: Cell lines		
CAPAN2	ATCC	Cat#HTB-80; RRID: CVCL_0026
PANC 10.05	ATCC	Cat#CRL-2547; RRID: CVCL_1639
PANC 03.27	ATCC	Cat#CRL-2549; RRID: CVCL_1635
HPAC	ATCC	Cat#CRL-2119; RRID: CVCL_3517
hTERT-HPNE (HPNE)	Gift from Steve Elledge	RRID: CVCL_C466
HPD	Abigail Miller	Furukawa et al.[27]
IMR-90	ATCC	Cat#CCL-186; RRID: CVCL_0347
BJ	ATCC	Cat#CRL-2522; RRID: CVCL_3653
MCF10A	Gift from Jayanta Debnath	Cat#CRL-10317; RRID: CVCL_0598
RPE-1	Clontech	no longer available
HEKa	ATCC	PCS-200-011
Experimental models: Organisms/strains		
Mouse: Nu/Nu laboratory mice for cell line- and patient-derived xenograft models	Charles River Laboratories	RRID:IMSR_CRL:088
Mouse: Pdx1-Cre; LSL-$Kras^{G12D/+}$; LSL-$Trp53^{R172H/+}$ (GEMM KPC model)	Hingorani et al.[37]	N/A
Oligonucleotides		
ON-TARGETplus SMARTpool Human MCL1 siRNA	Horizon Discovery (Dharmacon)	Cat#L004501-00-0005
ON-TARGETplus Non-targeting Control Pool	Horizon Discovery (Dharmacon)	Cat#D-001810-10-50
ON-TARGETplus SMARTpool Human USP9X siRNA	Horizon Discovery (Dharmacon)	Cat#L-006099-00-0005
MCL1 Forward: 5′-GAAAGCTGCATCGAACCATTAG-3′	Invitrogen	N/A
MCL1 Reverse: 5′- AGAACTCCACAAACCCATCC-3′	Invitrogen	N/A
UBC Forward: 5′- ATTTGGGTCGCGGTTCTTG-3′	Invitrogen	N/A
UBC Reverse: 5′- TGCCTTGACATTCTCGATGGT-3′	Invitrogen	N/A

(*Continued on next page*)

Please cite this article in press as: Perurena et al., USP9X mediates an acute adaptive response to MAPK suppression in pancreatic cancer but creates multiple actionable therapeutic vulnerabilities, Cell Reports Medicine (2023), https://doi.org/10.1016/j.xcrm.2023.101007

CellPress
OPEN ACCESS

Continued

REAGENT or RESOURCE	SOURCE	IDENTIFIER
Recombinant DNA		
N-HA-FLAG-pHAGE-GFP-Puro	Gift from Wade Harper	N/A
N-HA-FLAG-pHAGE-MCL1-Puro	MCL1 was cloned into the backbone provided by Wade Harper	pDONR221 MCL1 Cat#HsCD00042645
pRK5-HA-Ubiquitin-WT	Gift from Ted Dawson	RRID: Addgene_17608
pLKO.1-shCtrl-Puro Target sequence: 5′-CCTAAGGTTAA GTCGCCCTCG-3′	Addgene	RRID: Addgene_136035
pLKO.1-shUSP9X_1-Puro Target sequence: 5′-GAGAGTTTATTCACTGTCTTA-3′	Sigma-Aldrich	TRCN0000007361
pLKO.1-shUSP9X_2-Puro Target sequence: 5-CGCCTGATTCTTCCAATGAAA-3′	Sigma-Aldrich	TRCN0000007364
pLKO.1-shUSP9X_3-Puro Target sequence: 5′-CACCTCAAACCAAGGATCAA-3′	Sigma-Aldrich	TRCN0000011091
pLKO.1-shMCL1-Puro Target sequence: 5′-GCCTAGTTTATCACCAATAAT-3′	Sigma-Aldrich	TRCN0000196390
LV05 U6-sgCtrl:EF1-Cas9+FLAG-2A-Puro Target sequence: 5′-CGCGATAGCGCGAATATATT-3′	Sigma-Aldrich	Clone ID#NegativeControl1
LV05 U6-sgBIM:EF1-Cas9+FLAG-2A-Puro Target sequence: 5′-CTGCAATTGTCTACCTTCT-3′	Sigma-Aldrich	Clone ID#HSPD0000059472
LV05 U6-sgMCL1:EF1-Cas9+FLAG-2A-Puro Target sequence: 5′-GGACCTCGGCGCCAATGGG-3′	Sigma-Aldrich	CloneID# HSPD0000025257
Software and algorithms		
GraphPad Prism v9.2.0	GraphPad	RRID: SCR_002798
Incucyte S3 Software v2021A	Sartorius	RRID: SCR_019874
Cancer Dependency Map Portal (DepMap) (https://depmap.org/portal/gene/MCL1?tab=dependency&dependency=Chronos_Combined)	Broad Institute	RRID: SCR_017655
ImageJ Software v1.5a	ImageJ	RRID:SCR_003070
SynergyFinder	University of Helsinki	RRID:SCR_019318

RESOURCE AVAILABILITY

Lead contact

Further information and requests for resources and reagents should be directed to and will be fulfilled by the lead contact, Karen Cichowski (kcichowski@bwh.harvard.edu).

Materials availability

All unique reagents generated in this study are available from the lead contact and may require a completed Materials Transfer Agreement.

Data and code availability

- This paper analyzes existing CRISPR (DepMap 22Q2 Public+Score, Chronos) data, publicly accessible through the Broad Institute at depmap.org.
- This paper does not report original code.
- Any additional information required to reanalyze the data reported in this paper is available from the lead contact upon request.

EXPERIMENTAL MODEL AND SUBJECT DETAILS

Human specimens

Patient-derived organoid cultures were initiated and maintained as previously described[31,46,47] from tumor biopsies obtained from patients receiving care at Dana-Farber Cancer Institute and the Brigham and Women's Hospital. Investigators obtained written,

Please cite this article in press as: Perurena et al., USP9X mediates an acute adaptive response to MAPK suppression in pancreatic cancer but creates multiple actionable therapeutic vulnerabilities, Cell Reports Medicine (2023), https://doi.org/10.1016/j.xcrm.2023.101007

informed consent from patients at least 18 years old and diagnosed with pancreatic cancer for Dana-Farber/Harvard Cancer Center Institutional Review Board (IRB)-approved protocols 11-104, 17-000, 03-189, and/or 14-408 for tissue collection, molecular analysis, and organoid generation. Organoids used in this manuscript were derived from metastatic specimens from three female and one male patient and were collected after patients had been treated and progressed on at least one chemotherapy regimen. PCA 41 PDX tumors were generated from a 60-year-old male, with no previous treatments, at Dana-Farber Cancer Institute from IRB-approved protocol 03-189 and written informed patient consent. More information is listed below in method details.

Animals

Cell line-derived xenograft experiments and the PDX experiment were approved by the Center for Animal and Comparative Medicine at Brigham and Women's Hospital and by Dana-Farber Cancer Institute, respectively, in accordance with the NIH Guidelines for the Care and Use of Laboratory Animals and the Animal Welfare Act. These experiments were performed in female athymic Nu/Nu mice 6-8 weeks old purchased from Charles Laboratories. The experiment with KPC GEMM mice (Pdx1-Cre; LSL-Kras$^{G12D/+}$; LSL-Trp53$^{R172H/+}$)[37] was performed at The Beatson Institute for Cancer Research (UK). Mice on a mixed background were bred in-house and maintained in conventional caging with environmental enrichment, access to standard chow and water *ad libitum*. Mice of both sexes were recruited onto study. All experiments were performed in accordance with UK Home Office regulations (under project licence 70/8375), with approval from the University of Glasgow Animal Welfare and Ethical Review Board and adhered to ARRIVE guidelines. More information is listed below in method details.

Cell lines

CAPAN2, PANC 10.05, PANC 03.27, HPAC, IMR-90, BJ and HEKa (primary epidermal keratinocytes, adult) cell lines were purchased from ATCC. RPE-1 cells were purchased from Clontech. hTERT-HPNE (HPNE) cells were provided by Dr. Steve Elledge. MCF10A cells were provided by Dr. Jayanta Debnath. HPD cells[27] were provided by Dr. Abigail Miller. PANC 10.05 and PANC 03.27 cells were grown in RPMI supplemented with 10% FBS, Penicillin-Streptomycin and L-glutamine. CAPAN2 cells were grown in McCoy's 5A supplemented with 10% FBS, Penicillin-Streptomycin and L-glutamine. HPAC, HPD and RPE-1 cells were grown in DMEM supplemented with 10% FBS, Penicillin-Streptomycin and L-glutamine. IMR-90 and BJ cells were grown in EMEM supplemented with 10% FBS, Penicillin-Streptomycin and L-glutamine. HPNE cells were grown in 75% DMEM and 25% M3 Base Medium (Incell Corp., #M300F) supplemented with 10% FBS, Penicillin-Streptomycin and L-glutamine. MCF10A cells were grown in DMEM/F12 supplemented with 5% horse serum, Penicillin-Streptomycin, 20 ng/ml EGF, 0.5 μg/ml hydrocortisone, 100 ng/ml cholera toxin and 10 μg/ml insulin. HEKa cells were grown in Dermal Cell Basal Medium (ATCC, #50-189-650FP) supplemented with a keratinocyte growth kit (ATCC, #50-189-651FP). All cell lines were grown at 37°C and 5% CO_2.

METHOD DETAILS

Drugs

Trametinib (*in vitro*), MK2206, AZD2014 and EOAI3402143 were purchased from Selleck Chemicals. Trametinib used for *in vivo* experiments was purchased from LC Laboratories. S63845 and AMG-176 were purchased from Chemietek. MG132 was used at a final concentration of 10 μM where indicated and was purchased from Millipore (#474790). Cycloheximide was used at a final concentration of 25 μg/ml where indicated and was purchased from Sigma (#C7698). THZ1 was purchased from MedChemExpress. THZ531 was provided by Dr. Nathanael Gray. Drug concentrations are specified in each figure.

Incucyte analysis of caspase activation and cell counts

Cells were seeded at 3,000-5,000 cells/well in 96-well clear bottom black plates (ThermoScientific, #165305). Nuclei were labeled by either stably expressing Incucyte Nuclight Red (Sartorius, #4625) or by transient labeling with Incucyte Nuclight Rapid Red Reagent (Sartorius, #4717). 24 hours after seeding (time zero) media was replaced with media containing the indicated compounds and CellEvent Caspase-3/7 Green Detection Reagent (Invitrogen, #C10423) at a final dilution of 1:1000 to detect caspase-3/7-mediated cleavage and activation. Staurosporine (Sigma, #S5921) and etoposide (Sigma, #341205) were used as positive controls. Four images per well were acquired at 10X in phase, green (300 ms acquisition time), and red (400 ms acquisition time) channels every 2-4 hours using an Incucyte S3 imager. Instrument set-up for image acquisition and image analysis was performed using Incucyte S3 software (v2021A). To determine the percentage of caspase-3/7+ cells, overlap (red and green) counts/well were normalized to red counts/well at each timepoint. To calculate changes in cell number, for each well red counts/well at each timepoint were normalized to time zero red counts in that well. For long-term assays in Figure S3C, no CellEvent Caspase-3/7 Green Detection Reagent was added and media with drugs was replaced every 3-4 days.

Cell counting data

Cells were plated at 1.0-1.5x10^5 cells/well in 6-well plates in technical triplicates (one triplicate per treatment arm per time point and an additional triplicate to obtain day 0 counts). 24 hours after seeding (day 0) cells (one triplicate) were trypsinized, spun down and manually counted in a hemocytometer. Immediately after, indicated compounds were added to the remaining triplicates by replacing media. At day 3 (in log2 fold change bar graphs) or at day 3, 6 and 9 (log2 fold change over time graphs) cells were trypsinized, spun

Please cite this article in press as: Perurena et al., USP9X mediates an acute adaptive response to MAPK suppression in pancreatic cancer but creates multiple actionable therapeutic vulnerabilities, Cell Reports Medicine (2023), https://doi.org/10.1016/j.xcrm.2023.101007

down and manually counted in a hemocytometer. Final cell counts at each time point were normalized to day 0 counts to determine the change in cell number over the experiment and log2 transformed for graphical representation.

Crystal violet staining assays

Cells were seeded at 50,000-150,000 cells/well in 12-well plates. Next day, media was replaced with fresh media containing the indicated drugs. Media + drugs were replaced at day 3 or 4. At day 7, cells were washed twice with PBS, fixed in 10% formalin diluted 1:2 in PBS for 15 min and stained with 0.02% crystal violet for 30 min – 2 h. Stained wells were washed with deionized water and scanned. For quantification, crystal violet in each replicate was solubilized in 20% acetic acid. Absorbance of diluted samples was measured at 570 nm and normalized to DMSO.

In vitro pre-treatment experiments

For trametinib pre-treatment experiments, 24 h after seeding, cells were treated with DMSO (control) or trametinib for 48 h. At that point (time 0), media in DMSO-treated wells was replaced with media containing DMSO or THZ1 (or S63845) and media in trametinib-treated wells was replaced with media containing trametinib or trametinib + THZ1 (or S63845).

Transfections and infections

si*MCL1* (#L004501-00-0005), si*USP9X* (L-006099-00-0005) and non-targeting siRNA (#D-001810-10-50) ON-TARGETplus smart pools were purchased from Dharmacon. Cells were transfected for 6 hours in antibiotic free media with 50 nM siRNA, in the presence of Lipofectamine RNAiMAX Transfection Reagent (Invitrogen, #13778150) at 1:400 dilution. PLKO.1 shRNA plasmids with the following target sequences were purchased from Sigma: shUSP9X_1 TRCN0000007361 (5′-GAGAGTTTATTCACTGTCTTA-3′), shUSP9X_2 TRCN0000007364 (5′- CGCCTGATTCTTCCAATGAAA-3′), shUSP9X_3 TRCN0000011091 (5′- CACCTCAAACCAAGG ATCAA-3′) and shMCL1 TRCN0000196390 (5′-GCCTAGTTTATCACCAATAAT-3′). A control shRNA (shCNT) was purchased from Addgene (5′-CCTAAGGTTAAGTCGCCCTCG-3′). CRISPR LV05 U6-sgRNA:EF1-Cas9+FLAG-2A-Puro guides with the following target sequences were purchased from Sigma-Aldrich: sgCtrl (Clone NegativeControl1, 5′-CGCGATAGCGCGAATATATT-3′), sgMCL1 (Clone HSPD0000025257, 5′-GGACCTCGGCGCCAATGGG-3′) and sgBIM (Clone HSPD0000059472, 5′- CTGCAA TTGTCTACCTTCT-3′). Lentivirus was produced in 293T cells using x-TremeGENE 9 DNA Transfection Reagent (Roche, #6365787001) and collected 48 hours after transfection. Cells were infected for 16 hours with virus at 1:4 dilution in the presence of 8 μg/ml polybrene. Cells were recovered from infection for 24 hours and selected in 1-2 μg/ml puromycin for 3-4 days. pRK5-HA-Ubiquitin-WT was a gift from Ted Dawson (RRID: Addgene_17608). For HA-Ub IPs, cells seeded in 15-cm plates were transfected with 18 μg of the plasmid with x-TremeGENE 9 DNA Transfection Reagent (Roche, #6365787001) for 6 hours.

RNA extraction and quantitative PCR

Total RNA was isolated with RNeasy Plus Mini kit (Qiagen, #74136) and retrotranscribed with qScript cDNA synthesis kit (QuantaBio, #95047-500), following manufacturer's instructions. PerfeCTa SYBR Green SuperMix Reagent (QuantaBio, #95054-500) was used for quantitative PCR amplification and reactions were run on a Bio-Rad CFX96 cycler in technical triplicates. mRNA levels were determined based on a standard curve for each primer set. The following are the primer sequences used for amplification: MCL1 For: 5′-GAAAGCTGCATCGAACCATTAG-3′; MCL1 Rev: 5′-AGAACTCCACAAACCCATCC-3′; UBC For: 5′-ATTTGGGTCGCGGTTC TTG-3′; UBC Rev: 5′-TGCCTTGACATTCTCGATGGT-3′.

Western blotting

Cells were lysed by scraping in boiling 1% SDS lysis buffer (10 mM Tris pH 7.5, 100 mM NaCl, 1% SDS), immediately boiled for 10 minutes, and frozen at -20°C. Tumors were collected in dry ice, crushed, syringed in boiling 1% SDS lysis buffer and boiled for 10 min. Protein concentrations were measured using BCA Protein Assay (Pierce, #23225). 15-30 μg of protein per condition were loaded into SDS-PAGE polyacrylamide gels and transferred onto PVDF membranes (Millipore, #IPVH00010). Membranes were blocked for 30-60 min in 5% milk in TBST buffer and incubated with primary antibodies overnight at 4°C. The following antibodies were used for detection: antibodies against Mcl-1 (#5453, #94296), Bcl-xL (#2762 and #2764), Bim (#2819), Bak (#12105), Bax (#2772), p-ERK (#4370), ERK (#9102), Vinculin (#4650), p-AKT (#4060), AKT (#9272), p-S6 ribosomal protein (#2215), S6 ribosomal protein (#2217), p-p70 S6 kinase (#9205), p70 S6 kinase (#9202), Bcl-2 (#2872) and USP9X (#14898) were purchased from Cell Signaling Technology. Antibodies against Mcl-1 (#ab32087) and total RNA Pol II (#ab817) were purchased from Abcam. Antibodies against p-S2 CTD Pol II (#04-1571), p-S5 CTD Pol II (#04-1572), and p-S7 CTD Pol II (#1570) were purchased from EMD Millipore. Antibody against alpha-Tubulin (#T5168) was purchased from Sigma.

Cycloheximide degradation assay

Cells were pre-treated with DMSO (control) or trametinib for up to 48 hours. At intervals up to 120 minutes prior to lysis cycloheximide was added to cells at a final concentration of 25 μg/ml to block translation. Levels of Mcl-1 and loading control were determined by western blot and Mcl-1 levels were quantified and normalized to loading control using ImageJ Software (v1.5a). Normalized Mcl-1 levels were natural log transformed to linearize the data.

Please cite this article in press as: Perurena et al., USP9X mediates an acute adaptive response to MAPK suppression in pancreatic cancer but creates multiple actionable therapeutic vulnerabilities, Cell Reports Medicine (2023), https://doi.org/10.1016/j.xcrm.2023.101007

Immunoprecipitation of Mcl-1 and Bim to detect complexes

Cells were lysed in NP40 lysis buffer (0.5% NP40, 50 mM Tris pH 8, 120 mM NaCl, with the addition of PhosSTOP phosphatase inhibitor tablets (Roche, #4906845001) and cOmplete Mini EDTA-free Protease Inhibitor Cocktail (Roche, #11836170001). 250 μg of total lysate was incubated with 2.5 μl Bim antibody (Cell Signaling, #2819), 1 μg Mcl-1 antibody (Santa Cruz, #sc-12756), normal rabbit IgG (Millipore, #12-370) or normal mouse IgG (Millipore, #12-371) overnight at 4°C. The following day 50 μl of Protein A (Pierce, #88846) or Protein G (Pierce, #88847) magnetic beads were incubated with lysates for 1 hour for Bim IP and Mcl-1 IP, respectively. Beads were washed 3 times with lysis buffer and incubated in 2x sample buffer for 15 min at room temperature. Eluted proteins were separated from the beads and boiled for 10 min. For Bim IP, anti-USP9X Cell Signaling #14898, anti-Mcl-1 Cell Signaling #5453 and anti-Bim Cell Signaling #2819 antibodies were used for western blot detection. For Mcl-1 IP, anti-Mcl-1 Abcam #ab32087 and anti-Bim Cell Signaling #2819 antibodies were used for western blot detection.

Immunoprecipitation of Mcl-1 and USP9X for Mcl-1:USP9X interaction

Cells were lysed using 1% CHAPS lysis buffer (1% CHAPS, 50 mM HEPES pH 7.5, 150 mM NaCl, 1% Triton X-100, 1 mM EDTA, 10 mM sodium pyrophosphate, 10 mM NaF, 2 mM Na_3VO_4, and complete Mini EDTA-free Protease Inhibitor Cocktail (Roche, #11836170001)). For the Mcl-1 IP, 1 mg of lysate was incubated with 2 μg rabbit anti-Mcl-1 (Santa Cruz, #sc-819) or normal rabbit IgG (Millipore, #12-370) and 50 μl Protein A magnetic beads (Pierce, #88846) for 3 h at 4°C. For the USP9X IP, 1.5 mg of lysate was incubated with 2 μg mouse anti-USP9X (Abnova, H00008239-M01) or normal mouse IgG (Millipore, #12-371) and 50 μl slurry Protein G magnetic beads (Pierce, #88847) for 3 h at 4°C. Beads were washed 3 times with lysis buffer containing 0.2% CHAPS and incubated in 2x sample buffer for 15 min at room temperature. Eluted proteins were separated from the beads and boiled for 10 min. For the Mcl-1 IP, anti-USP9X Cell Signaling #14898 and anti-Mcl-1 Abcam #ab32087 were used for western blot detection and for the USP9X IP, anti-Mcl-1 Cell Signaling #5453 and anti-USP9X Cell signaling #14898 were used for western blot detection.

Mcl-1 ubiquitination assay

PANC 10.05 and CAPAN2 cells were transfected with pRK5-HA-Ubiquitin-WT (gift from Ted Dawson, RRID: Addgene_17608). 24 hours after transfection, cells were treated with trametinib or DMSO (control) +/- 10 μM MG132 2 h prior to lysis. Cells were lysed in RIPA buffer (0.1% SDS, 1.0% Triton-X 100, 150 mM NaCl, 0.5% sodium deoxycholate, 50 mM Tris pH 8.0) containing PhosSTOP phosphatase inhibitor tablets (Roche, #4906845001), cOmplete Mini EDTA-free Protease Inhibitor Cocktail (Roche, #11836170001) and 100 mM N-Ethylmaleimide (NEM). 1 mg of total protein was incubated with anti-HA magnetic beads (Pierce, #88836) for 2 h. Beads were washed 3 times with lysis buffer and incubated in 2x sample buffer for 15 min at room temperature. Eluted proteins were separated from the beads and boiled for 10 min. Anti-Mcl-1 Cell Signaling #94296 was used for immunoblots.

Initiation and culture of human patient-derived pancreatic cancer organoid models

As previously described,[31,47] biopsy specimens were minced with a scalpel and digested at 37°C for approximately 20 minutes using digest solution containing human complete organoid medium (see below), 1 mg/ml collagenase XI (Sigma Aldrich), 10 mg/ml DNase (Stem Cell Technologies), and 10 mM Y27632 (Selleck). After digestion and multiple washes, dissociated cells were seeded in 3-dimensional (3D) Growth-factor Reduced Matrigel (Corning), fed with human complete organoid medium containing advanced DMEM/F12 (Gibco), 10 mM HEPES (Gibco), 1x GlutaMAX (Gibco), 500 nM A83-01 (Tocris), 50 ng/ml mEGF (Peprotech), 100 ng/ml mNoggin (Peprotech), 100 ng/ml hFGF10 (Peprotech), 10 nM hGastrin I (Sigma), 1.25 mM N-acetylcysteine (Sigma), 10 mM Nicotinamide (Sigma), 1x B27 supplement (Gibco), R-spondin1 conditioned media 10% final, Wnt3A conditioned media 50% final, 100 U/ml penicillin/streptomycin (Gibco), and 1x Primocin (Invivogen). Cultures were maintained at 37°C in 5% CO_2. 10 mM Y27632 (Selleck) was included in the culture medium of newly initiated samples until the first media exchange. For propagation, organoids were dissociated with TrypLE Express (Gibco) before re-seeding into fresh Matrigel and complete organoid culture medium. The identity of organoid models was authenticated by comparison of organoid whole genome sequencing with targeted genomic sequencing and CNV profiles of matched patient tissue and earlier passage models. Organoid cultures were routinely tested for mycoplasma contamination.

Patient-derived organoid compound testing and western blotting

For compound testing, organoids were dissociated to single cells. 1,000 viable cells were seeded into each well of ultra-low attachment 384-well plates (Corning) with 20 μl of complete medium containing 10% Matrigel. After 24 hours (day 0), cells were treated with DMSO (control) and an array of combinatorial doses of trametinib and S63845. After 5 days in culture with therapeutic agents, cell numbers were indirectly assessed by adding 20 μl of CellTiter-Glo 3D to each well, incubating for 1 hour at room temperature on a shaker, and measuring luminescence using an EnVision plate reader. Each condition was performed in triplicate, and each dose point was normalized to DMSO (control) to estimate relative cell number. At least 2 independent experiments were performed for each compound and organoid condition. Synergy scores were calculated using SynergyFinder. To collect protein lysates, 500,000 cells were seeded in suspension in media with 10% Matrigel. After 24 h (day 0), DMSO or drugs were added. At 48-72 h of treatment, organoids were pelleted, washed twice with cold PBS and resuspended in boiling 1% SDS lysis buffer as described above to prepare lysates.

Please cite this article in press as: Perurena et al., USP9X mediates an acute adaptive response to MAPK suppression in pancreatic cancer but creates multiple actionable therapeutic vulnerabilities, Cell Reports Medicine (2023), https://doi.org/10.1016/j.xcrm.2023.101007

CellPress
OPEN ACCESS

Cell line-derived xenografts

Animal procedures were approved by the Center for Animal and Comparative Medicine at Brigham and Women's Hospital in accordance with the NIH Guidelines for the Care and Use of Laboratory Animals and the Animal Welfare Act (Protocol #2016N000467). Female athymic Nu/Nu mice 6-8 weeks of age were purchased from Charles River Laboratory. $2x10^6$ CAPAN2 and $3x10^6$ PANC 03.27 cells, resuspended in 50:50 PBS:Matrigel, were subcutaneously injected into each rear flank. Mice were randomized and enrolled in treatment groups when tumors reached 130-200 mm^3. Tumors were measured with vernier calipers and tumor volume was calculated using the standard formula $L \times W^2 \times 0.52$.

Human PDX model

The PCA 41 PDX study was performed at Dana-Farber Cancer Institute in accordance with the NIH Guidelines for the Care and Use of Laboratory Animals and the Animal Welfare Act. Tumor fragments (2x2x2 mm) were implanted into female athymic Nu/Nu mice (Charles Laboratory). Mice were randomized and enrolled in treatment groups when tumors reached 130-200 mm^3. Tumors were measured with vernier calipers and tumor volume was calculated using the standard formula $L \times W^2 \times 0.52$.

KPC GEMM experiment

The GEMM experiment was performed at The Beatson Institute for Cancer Research (UK) in accordance with UK Home Office regulations (under project licence 70/8375), with approval from the University of Glasgow Animal Welfare and Ethical Review Board and adhered to ARRIVE guidelines. Mice were enrolled when a palpable tumor was detected (approximately 4-6 mm) and was confirmed to be less than 750 mm^3 by ultrasound. Mice were monitored by body score and ultrasound once a week until mice reached endpoint according to institutional guidelines.

In vivo drug treatments

Mice were treated once daily (QD) with trametinib by oral gavage at 0.6 mg/kg. Trametinib was prepared in 0.5% hydroxypropyl methylcellulose (Sigma, #H7509)/0.2% Tween-80, pH 8.0. Mice were treated with THZ1 twice daily (BID) for 5 days/week and once daily (QD) for two days/week by i.p injection at 10 mg/kg. THZ1 was prepared in 10% DMSO in 5% Dextrose (D5W). S63845 was prepared in sterile 2% VitaminE/TPGS in 0.9% NaCl and administered at 30 mg/kg twice weekly by IV injection. For AMG-176 studies mice were pre-treated with either trametinib (0.6 mg/kg) or vehicle daily (QD). After 4 days of pre-treatment, vehicle-treated mice were treated with vehicle or 50 mg/kg AMG-176, while trametinib-treated mice were treated with trametinib or trametinib + AMG-176 daily (QD) for 6 days. AMG-176 was administered by oral gavage and was prepared extemporaneously in 25% hydroxypropyl-beta-cyclodextrin (pH 9.0) followed by vortexing and brief sonication.

Immunohistochemistry

Tumors were fixed in buffered formalin, stored in 70% ethanol, paraffin embedded and sectioned. Slides were stained with hematoxylin and eosin (H&E) or anti-cleaved caspase-3 (Cell Signaling, #9664) at 1:150 dilution. Images were captured at the indicated magnifications using a Nikon Eclipse TS100 microscope.

QUANTIFICATION AND STATISTICAL ANALYSIS

For quantitative measurements of caspase-3/7 activation over time, graphs represent the mean of indicated number of biological replicates ± SEM or technical replicates ± SD as indicated in figure legends. For all other quantitative measurements *in vitro*, graphs depict the mean of indicated number of technical replicates ± SD unless otherwise noted. *In vivo* tumor volume over time graphs represents the mean ± SEM. Waterfall plots were used to depict changes in individual tumor volume. Where indicated 2-tailed unpaired t-tests, ANOVA followed by Tukey's multiple comparisons test, Mann Whitney tests, or long-rank tests were used to compare experimental groups and *P* values are indicated. A *P* value equal to or less than 0.05 was considered significant. All data were graphed and analyzed using GraphPad Prism v9.2.0.

Cell Reports Medicine, Volume *4*

Supplemental information

USP9X mediates an acute adaptive response to MAPK suppression in pancreatic cancer but creates multiple actionable therapeutic vulnerabilities

Naiara Perurena, Rebecca Lock, Rachel A. Davis, Srivatsan Raghavan, Natalie F. Pilla, Raymond Ng, Patrick Loi, Caroline J. Guild, Abigail L. Miller, Ewa Sicinska, James M. Cleary, Douglas A. Rubinson, Brian M. Wolpin, Nathanael S. Gray, Sandro Santagata, William C. Hahn, Jennifer P. Morton, Owen J. Sansom, Andrew J. Aguirre, and Karen Cichowski

S1A

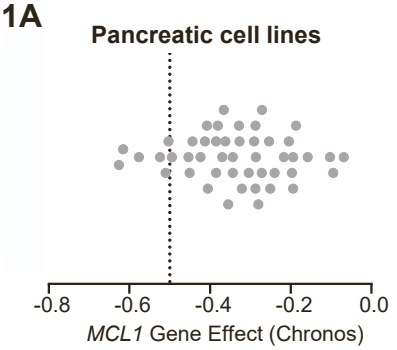

S1B

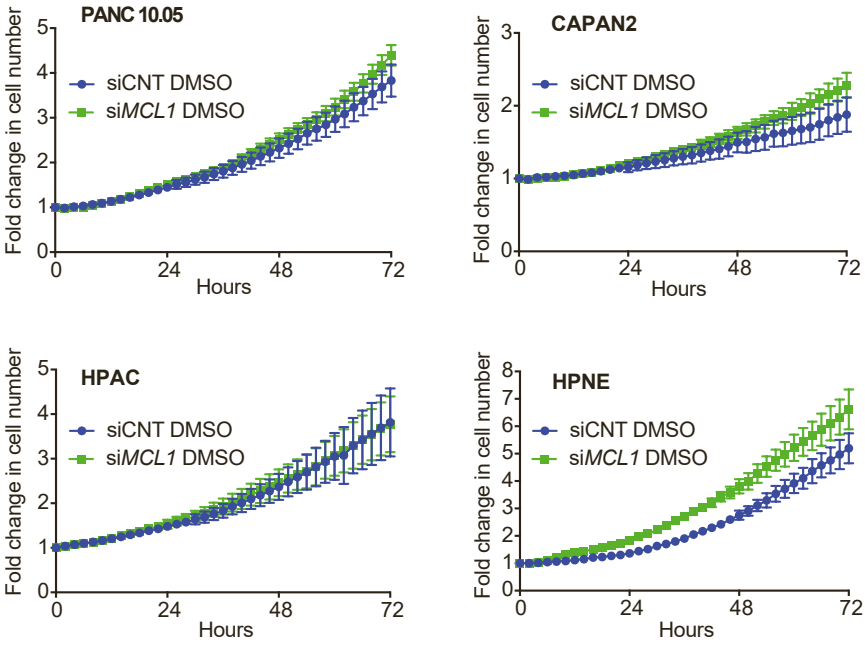

S1C

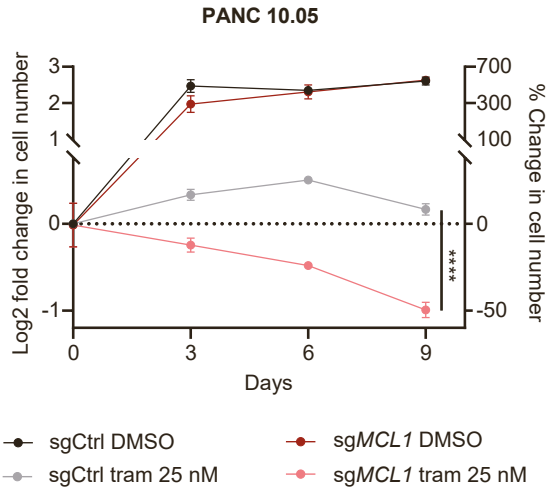

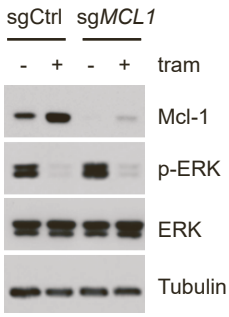

S1D

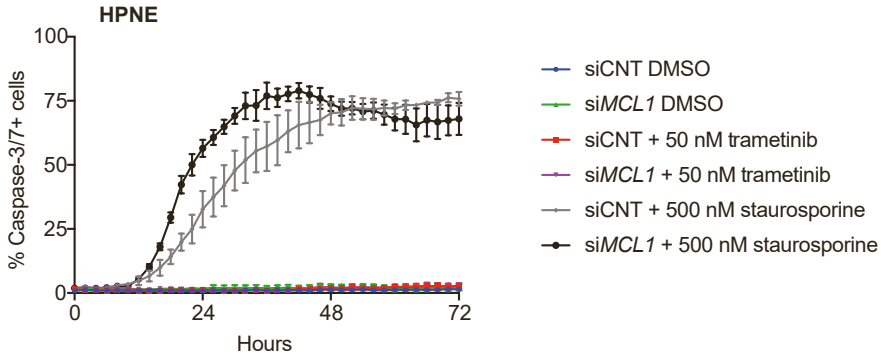

Figure S1. MEK inhibition sensitizes PDAC lines to Mcl-1 depletion (related to Figure 2).

(A) *MCL1* dependency scores in pancreatic cell lines. Each dot represents a single cell line. Cell lines with a dependency score of -0.5 or less are considered dependent. Data from CRISPR (DepMap 22Q2 Public+Score, Chronos), publicly accessible through the Broad Institute at depmap.org.

(B) Fold change in PDAC and HPNE cell number (red nuclei) over 72 h following transfection with siCNT or si*MCL1*, measured by Incucyte (mean ± SEM of biological replicates, n=4).

(C) Graph: Log2 fold change (left y-axis) and percent change (right y-axis) in cell number in sg*MCL1* or sgCtrl PANC 10.05 cells during 9 days of 25 nM trametinib treatment (mean ± SD of technical replicates, n=3; ****p<0.0001, unpaired t-test). Western blots: Levels of Mcl-1 in PANC 10.05 cells following sgRNA-mediated knockdown and treatment with 25 nM trametinib for 48 h.

(D) Levels of caspase-3/7 activation in si*MCL1* or siCNT HPNE cells treated with DMSO, 50 nM trametinib or 500 nM staurosporine as a positive control (mean ± SEM of biological replicates, DMSO and trametinib: n=4, staurosporine: n=3).

S2

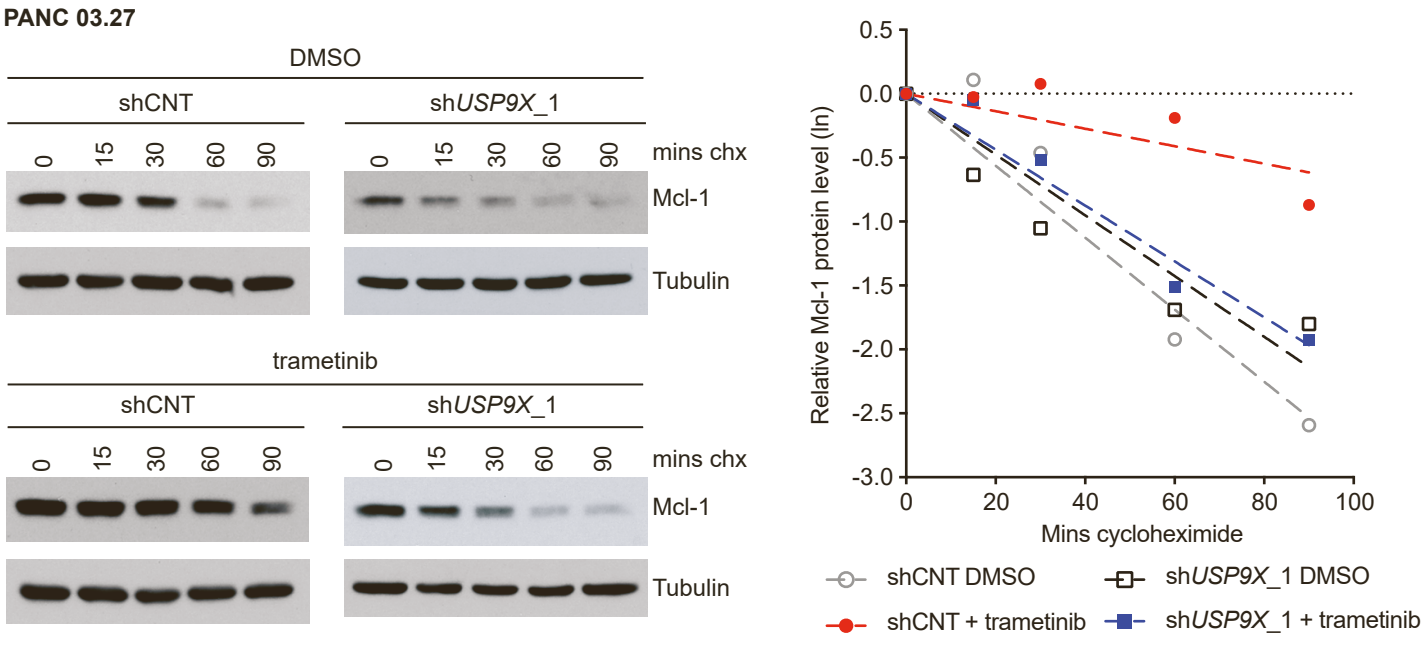
PANC 03.27
DMSO
shCNT
shUSP9X_1
0
15
30
60
90
mins chx
Mcl-1
Tubulin
trametinib
shCNT
shUSP9X_1
0
15
30
60
90
mins chx
Mcl-1
Tubulin
Relative Mcl-1 protein level (ln)
0.5
0.0
-0.5
-1.0
-1.5
-2.0
-2.5
-3.0
0
20
40
60
80
100
Mins cycloheximide
shCNT DMSO
shUSP9X_1 DMSO
shCNT + trametinib
shUSP9X_1 + trametinib

Figure S2. USP9X regulates Mcl-1 stability following MEK inhibition (related to Figure 4).

Western blots: Mcl-1 protein levels in PANC 03.27 cells expressing shCNT or sh*USP9X* treated with DMSO (control) or 25 nM trametinib for 48 h prior to cycloheximide (chx) treatment for the indicated times. Graph: Natural log (ln) transformed quantification of Mcl-1 normalized to tubulin and relative to non-cycloheximide treated controls.

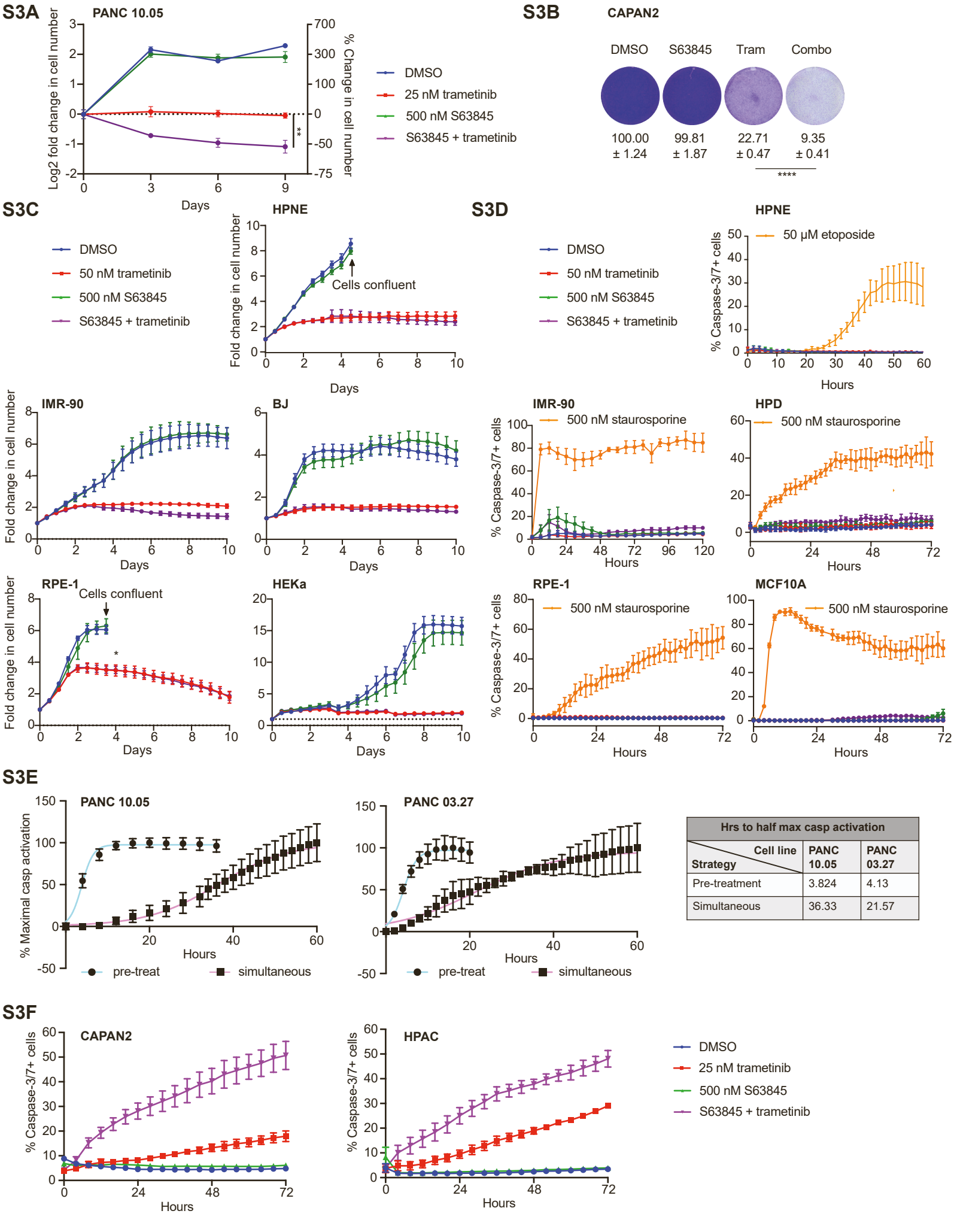
S3A
PANC 10.05
Log2 fold change in cell number
% Change in cell number
Days
DMSO
25 nM trametinib
500 nM S63845
S63845 + trametinib
**
S3B
CAPAN2
DMSO
S63845
Tram
Combo
100.00 ± 1.24
99.81 ± 1.87
22.71 ± 0.47
9.35 ± 0.41
****
S3C
DMSO
50 nM trametinib
500 nM S63845
S63845 + trametinib
HPNE
Fold change in cell number
Cells confluent
Days
IMR-90
BJ
RPE-1
HEKa
S3D
DMSO
50 nM trametinib
500 nM S63845
S63845 + trametinib
HPNE
50 µM etoposide
% Caspase-3/7+ cells
Hours
IMR-90
500 nM staurosporine
HPD
RPE-1
MCF10A
S3E
PANC 10.05
PANC 03.27
% Maximal casp activation
Hours
pre-treat
simultaneous
Hrs to half max casp activation
Strategy \ Cell line
PANC 10.05
PANC 03.27
Pre-treatment
3.824
4.13
Simultaneous
36.33
21.57
S3F
CAPAN2
HPAC
% Caspase-3/7+ cells
Hours
DMSO
25 nM trametinib
500 nM S63845
S63845 + trametinib

Figure S3. Mcl-1 inhibitors sensitize PDAC cells and patient derived tumor organoids to MEK inhibition (related to Figure 5).

(A) Graph depicting log2 fold change (left y-axis) and percent change (right y-axis) in cell number in PANC 10.05 cells treated with DMSO, 500 nM S63845, 25 nM trametinib (tram) and combination of both drugs for 9 days (mean ± SD of technical replicates, n=3, **p<0.01, unpaired t-test).

(B) Crystal violet staining of CAPAN2 cells treated with DMSO, 500 nM S63845, 25 nM trametinib (tram) or the combination of both drugs (combo) for 7 days. One representative image is shown per condition. Numbers indicate absorbance values relative to DMSO (mean ± SD, n=3; ****p<0.0001, unpaired t-test.

(C) Fold change in cell number, measured by monitoring red nuclei in Incucyte, over 10 days of treatment with DMSO, 50 nM trametinib, 500 nM S63845 or the combination of both drugs (mean ± SD of technical replicates, n=4-6) in the indicated cell lines. *Cells confluent due to increase in cell size with trametinib treatment.

(D) Kinetics of caspase-3/7 activation in cells treated with DMSO, 50 nM trametinib, 500 nM S63845 or the combination of both drugs. Etoposide and staurosporine were used as positive controls where indicated. Data are mean ± SD of technical replicates (n=4-6), except for HPNE (± SEM of 3 biological replicates).

(E) Graphs: Comparisons of the rate of caspase activation between trametinib pre-treatment followed by combination treatment and simultaneous dosing in PANC 10.05 and PANC 03.27 cells. Graphs represent data from the combination (trametinib + S63845) condition shown in Figures 5B and 5D, normalized to 100% for direct comparison. Table: Time to half-maximal caspase activation comparing trametinib pre-treatment and simultaneous treatment.

(F) Percentage of caspase-3/7+ cells in CAPAN2 and HPAC cell lines following trametinib pre-treatment and subsequent combination of 500 nM S63845 and 25 nM trametinib (mean ± SEM of biological replicates, n=4).

S4A

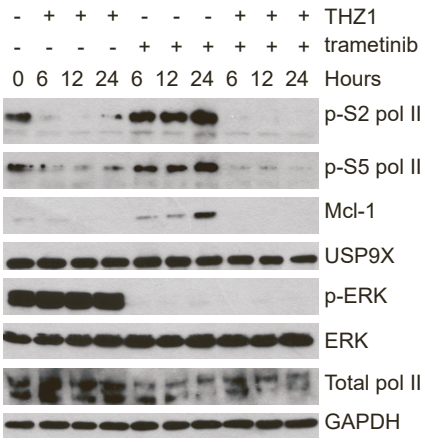

S4B

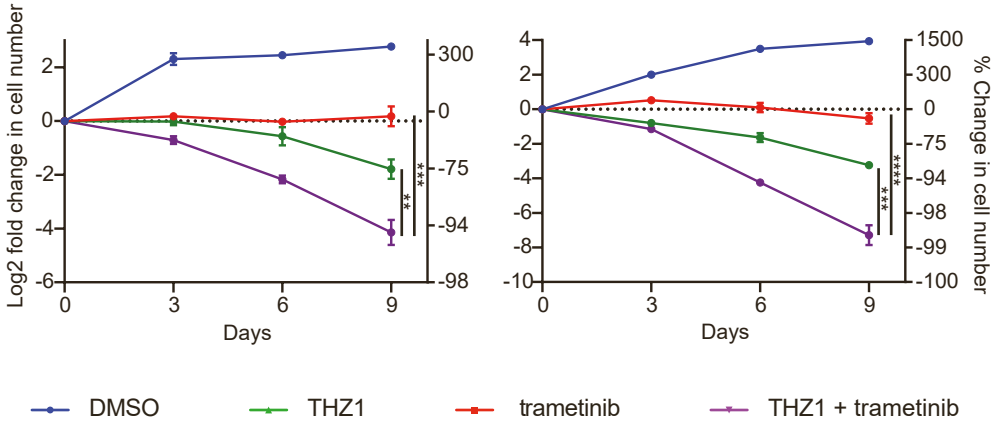

S4C

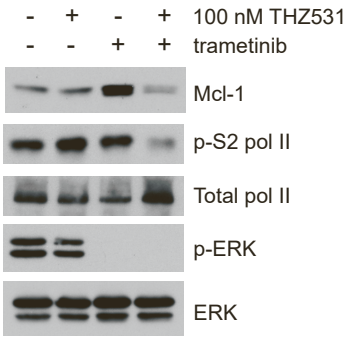

S4D

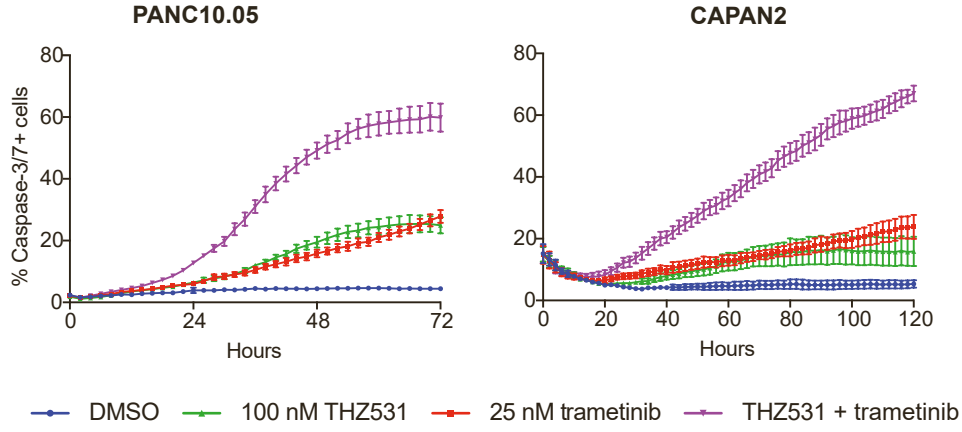

S4E

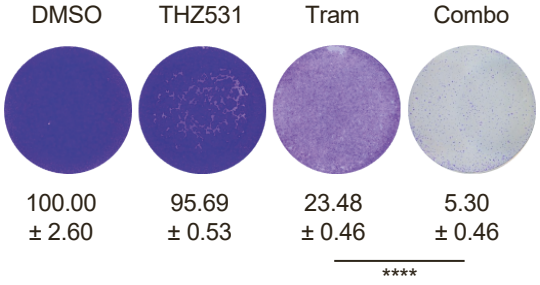

Figure S4. Transcriptional CDK inhibitors cooperate with trametinib in PDACs to reduce Mcl-1 levels and induce apoptosis (related to Figure 6).

(A) Western blots showing levels of Mcl-1, p-S2 pol II, p-S5 pol II and USP9X during a time course of 250 nM THZ1 and 25 nM trametinib treatment, alone or in combination, in PANC 10.05 cells.

(B) Graphs depicting log2 fold change (left y-axis) and corresponding percent change (right y-axis) in cell number in PANC 10.05 and CAPAN2 cells treated with DMSO, THZ1 (PANC 10.05: 100 nM, CAPAN2: 50 nM), 25 nM trametinib or the combination of both drugs (mean ± SD of technical replicates, n=3; **p<0.01, ***p<0.001, ****p<0.0001).

(C) Levels of Mcl-1 and p-S2 pol II in CAPAN2 cells pre-treated with DMSO (for DMSO and THZ531) or 25 nM trametinib (for trametinib and trametinib + THZ531) for 48 h followed by treatment with 100 nM THZ531 alone or in combination with 25 nM trametinib for 24 h.

(D) Percentage of caspase-3/7+ CAPAN2 and PANC 10.05 cells treated with 25 nM trametinib alone or in combination with 100 nM THZ531 (mean ± SEM of biological replicates, n=4).

(E) Crystal violet staining of CAPAN2 cells treated with DMSO, 100 nM THZ531, 25 nM trametinib (tram) or trametinib + THZ531 (combo). One representative image is shown per condition. Numbers indicate absorbance values relative to DMSO (mean ± SD, n=3; ****p<0.0001, unpaired t-test.